

# Development and genetics of red coloration in the zebrafish relative *Danio albolineatus*

Delai Huang<sup>1</sup>, Victor M Lewis<sup>1†</sup>, Tarah N Foster<sup>2</sup>, Matthew B Toomey<sup>2,3</sup>, Joseph C Corbo<sup>3</sup>, David M Parichy<sup>1,4\*</sup>

<sup>1</sup>Department of Biology, University of Virginia, Charlottesville, United States;

<sup>2</sup>Department of Biological Science, University of Tulsa, Tulsa, United States;

<sup>3</sup>Department of Pathology and Immunology, Washington University School of Medicine, St Louis, United States; <sup>4</sup>Department of Cell Biology, University of Virginia, Charlottesville, United States

**Abstract** Animal pigment patterns play important roles in behavior and, in many species, red coloration serves as an honest signal of individual quality in mate choice. Among *Danio* fishes, some species develop erythrophores, pigment cells that contain red ketocarotenoids, whereas other species, like zebrafish (*D. rerio*) only have yellow xanthophores. Here, we use pearl danio (*D. albolineatus*) to assess the developmental origin of erythrophores and their mechanisms of differentiation. We show that erythrophores in the fin of *D. albolineatus* share a common progenitor with xanthophores and maintain plasticity in cell fate even after differentiation. We further identify the predominant ketocarotenoids that confer red coloration to erythrophores and use reverse genetics to pinpoint genes required for the differentiation and maintenance of these cells. Our analyses are a first step toward defining the mechanisms underlying the development of erythrophore-mediated red coloration in *Danio* and reveal striking parallels with the mechanism of red coloration in birds.

\*For correspondence: dparichy@virginia.edu

Present address: <sup>†</sup>Institute of Molecular Biology, University of Oregon, Eugene, United States

Competing interest: The authors declare that no competing interests exist.

Funding: See page 18

Received: 11 May 2021

Preprinted: 22 May 2021

Accepted: 25 August 2021

Published: 26 August 2021

Reviewing Editor: Tanya T Whitfield, University of Sheffield, United Kingdom

© Copyright Huang et al. This article is distributed under the terms of the [Creative Commons Attribution License](https://creativecommons.org/licenses/by/4.0/), which permits unrestricted use and redistribution provided that the original author and source are credited.

## Introduction

Red and orange pigments deposited in the skin provide key signals that are subject to sexual or natural selection. For example, the intensity of red or orange coloration, or the area over which it occurs, has been associated with mating preferences in a variety of species (Milinski and Bakker, 1990; Hill, 1991; Houde, 1997; Grether, 2000; Takahashi, 2018; Ansai et al., 2021) and in some cases the very conspicuousness that makes an individual attractive can make it more vulnerable to predators (Endler, 1980; Godin and McDonough, 2003; Johnson and Candolin, 2017). Red or orange coloration can also be associated with aggressive interactions (Evans and Norris, 1996; Pryke and Griffith, 2006; Dijkstra et al., 2008) and warning coloration (Brodie and Brodie, 1980; Stevens and Ruxton, 2012).

Red, orange, and yellow coloration is often mediated by the accumulation of carotenoids, fat-soluble compounds that are synthesized by plants and some fungi and bacteria, and obtained by animals via their diet and then subsequently modified (Bagnara and Matsumoto, 2006; McGraw, 2006; Svensson and Wong, 2011; Sefc et al., 2014; Strange, 2016; Toews et al., 2017). More than a thousand naturally occurring carotenoids are known, and their basic structure consists of 40 carbon atoms derived from four terpene molecules (Figure 1A). Carotenoids contain a system of conjugated double bonds that absorb light in the visible range; the greater the length of the conjugated system, the more red-shifted the absorption. Yellow carotenoids, such as  $\beta$ -carotene or zeaxanthin, have a total of 11 conjugated double bonds, whereas red carotenoids, such as astaxanthin, have a total of 13 due to the addition of ketone groups in the 4 and 4' positions of the terminal rings of the molecule

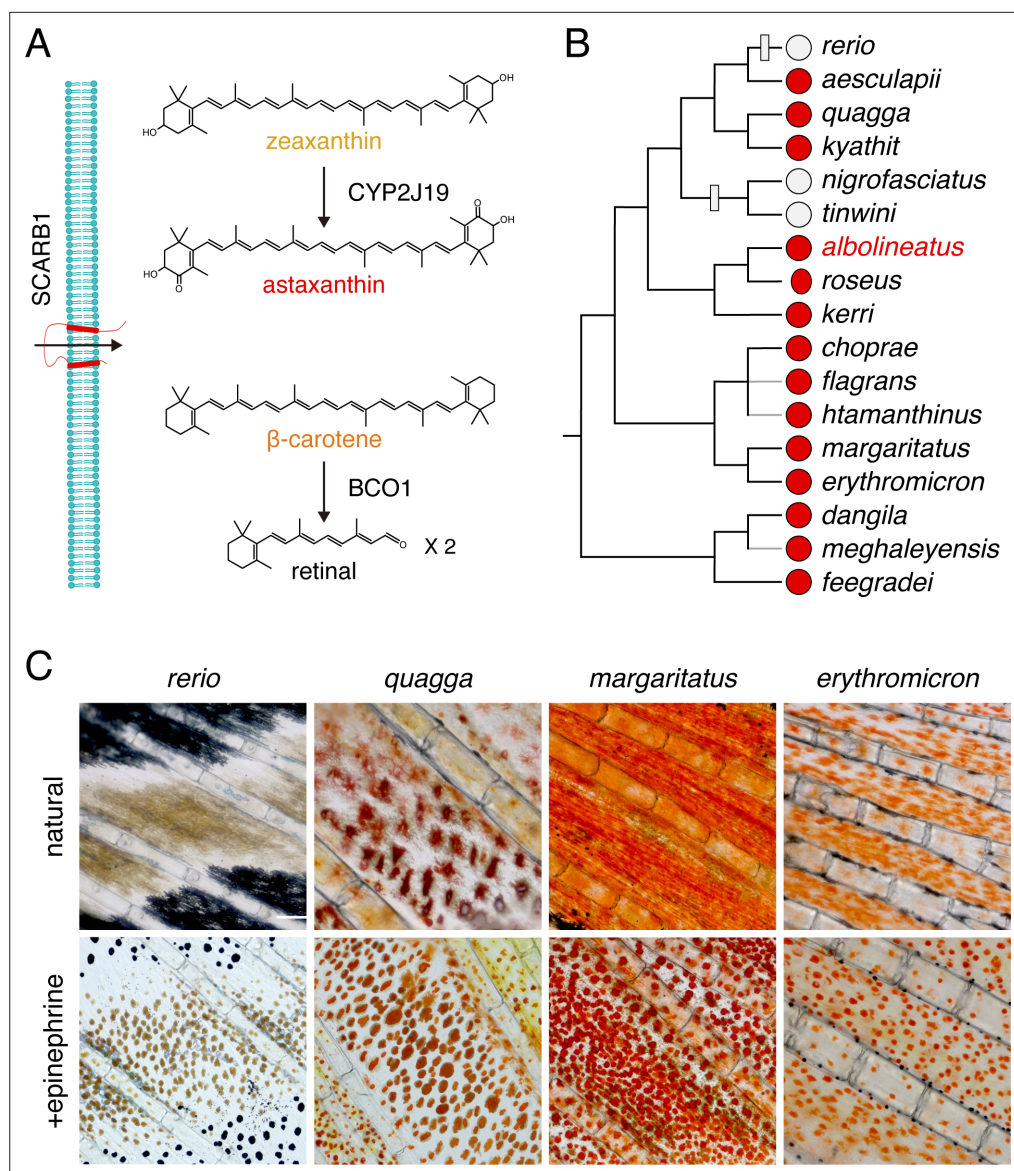


**Figure 1.** Carotenoid types and distribution of red erythrophores among *Danio* species. **(A)** Examples of major carotenoid types including yellow zeaxanthin, red astaxanthin, and orange  $\beta$ -carotene, with factors required for entry into cells and chemical modification (Main text). **(B)** Erythrophore presence (red circles) or absence (light gray circles) indicated by direct observation or prior species descriptions (Fang and Kottelat, 2000; Quigley et al., 2005; Engeszer et al., 2007; Kullander and Fang, 2009; Kullander, 2012; Kullander and Norén, 2016; Spiewak et al., 2018; McCluskey et al., 2021). A composite phylogeny based on several molecular evolutionary studies is shown; gray branches indicate lineage placements inferred by morphology alone (Tang et al., 2010; Kullander, 2012; Kullander et al., 2015; McCluskey and Postlethwait, 2015). Gray boxes across branches indicate lineages in which erythrophores are inferred most parsimoniously to have been lost. **(C)** Anal fin details of zebrafish (*rerio*) without erythrophores and other species with erythrophores. Cells are shown in their typical native states, with pigment dispersed, and following treatment with epinephrine, which causes pigment to be contracted toward cell centers. Scale bar: 100  $\mu$ m.

(Figure 1A). Many animal species possess endogenous ‘ketolase’ activity, and thus can add ketones to diet-derived yellow carotenoids to produce red ketocarotenoids. The final color displayed by an animal reflects the specific carotenoids absorbed in the gut, transported to peripheral tissues, and chemically modified to achieve specific light-absorptive properties. Carotenoids also have important functions as vitamin A precursors, as antioxidants, and as regulators of a variety of cellular functions. The multifunctionality of carotenoids, and the need to obtain them from the environment, have

contributed to the notion that carotenoids in the integument can serve as an honest signal of prospective fitness, to mates or rivals (Endler, 1980; Weaver et al., 2017; Weaver et al., 2018).

The cellular context for displaying carotenoid-dependent colors differs between endothermic and ectothermic vertebrates. In birds, carotenoids are concentrated in keratinocytes of the skin and displayed either directly or after incorporation into feathers (McGraw, 2006). In ectotherms, carotenoids are concentrated in lipid droplets within pigment cells, chromatophores, visible through the epidermis and dermis. Red chromatophores are known as erythrophores, whereas yellow or orange chromatophores are referred to as xanthophores. Besides accumulating carotenoids, both cell types can produce and retain pteridine pigments that sometimes also contribute to visible coloration (Schartl et al., 2016; Parichy, 2021).

Erythrophores and xanthophores, like other skin chromatophores—black melanophores, iridescent iridophores, and white leucophores—develop from embryonic neural crest cells, either directly, or indirectly, via latent progenitors in the peripheral nervous system or other tissue compartments (Kelsh et al., 2009; Patterson and Parichy, 2019). Though sharing a common cell lineage overall, the degree to which different chromatophore types share fate-restricted progenitors remains incompletely understood. In zebrafish for example, most xanthophores on the body differentiate as pteridine-containing xanthophores in the embryo, then proliferate and lose their color, only to reacquire carotenoid-dependent coloration in the adult; other xanthophores on the body and in the fin develop instead from latent progenitors (Tu and Johnson, 2011; McMenamín et al., 2014; Singh et al., 2016; Saunders et al., 2019). By contrast, the majority of adult iridophores and melanophores develop from a common progenitor in the peripheral nervous system (Budi et al., 2011; Dooley et al., 2013; Singh et al., 2016). Lineage relationships can be further complicated by direct transitions between chromatophore types. Such transitions have long been known to be inducible experimentally (Niu, 1954; Ide and Hama, 1976), but have also been found naturally in zebrafish, in which a class of fin leucophore develops directly from melanophores (Lewis et al., 2019).

With respect to red coloration, the lineage relationship of erythrophores to xanthophores is not known. Although studies across several species have revealed both similarities and differences in cytological appearance and pigment biochemistry (Matsumoto, 1965; Matsumoto and Obika, 1968; Ichikawa et al., 1998; Khoo et al., 2012; Djurdjevič et al., 2015), it remains unclear if erythrophores share a progenitor with xanthophores, or whether they might develop directly from xanthophores. Likewise, the genes required for red coloration, as opposed to orange or yellow coloration, remain largely unexplored, although two loci required for, or associated with, ketocarotenoid accumulation, have been identified in birds (Lopes et al., 2016; Mundy et al., 2016; Toomey et al., 2018).

Here, we exploit the presence of erythrophores in a zebrafish relative, the pearl danio *Danio albolineatus*, to interrogate cell lineage relationships between erythrophores and xanthophores, and to identify genes essential for red and orange coloration in this species. By clonal analysis and fate mapping we show that early erythrophores and xanthophores of the fin arise from a common, initially orange progenitor, the descendants of which adopt one or the other fate depending on their location. We further show that later-arising erythrophores and xanthophores of the fin develop directly from unpigmented precursors, and that transitions between erythrophore and xanthophore states can occur during regeneration. By screening candidate genes identified through transcriptomic comparisons of erythrophore- and xanthophore-containing fin tissues, we additionally demonstrate requirements for several genes in red or yellow coloration. These include loci encoding a cytochrome P450 monooxygenase, belonging to the same protein family as an enzyme previously implicated in avian red coloration (Lopes et al., 2016), as well as two genes not previously implicated in red coloration. These results lay the groundwork for future biochemical analyses of carotenoid processing, dissection of mechanisms of erythrophore fate specification, and comparative analyses of species-specific losses or gains of erythrophore-dependent coloration.

## Results

### Phylogenetic distribution of erythrophores in *Danio* and patterning of erythrophores and xanthophores in the anal fin of *D. Albolineatus*

The adult zebrafish (*Danio rerio*) pigment pattern includes yellow xanthophores, black melanophores, at least three types of iridescent iridophores, and two types of white cells (melanoleucophores and

xantholeucophores) (Hirata et al., 2003; Lewis et al., 2019; Patterson and Parichy, 2019; Gur et al., 2020). Zebrafish does not have red erythrophores. Because erythrophores occur in many other species of teleosts, we surveyed the distribution of these cells across the *Danio* genus more broadly. Of 17 *Danio* species assessed, 14 had erythrophores indicating this cell type is common and most likely was present in the common ancestor of all *Danio* species (Figure 1B–D).

We focused on *D. albolineatus* since erythrophores are abundant in this species and are separated spatially from other pigment cells, an arrangement likely to facilitate analysis (Goodrich and Greene, 1959). In the anal fin of adults, red erythrophores were located proximally and were separated from the more distal yellow xanthophores by a narrow stripe of melanophores (Figure 2A). Although erythrophores were present in both sexes, the cells were more deeply and consistently red in males than females and we therefore focused on males at stages when sexes were distinguishable (Figure 2—figure supplement 1A). Male fish older than 1 year often lacked fin stripe melanophores, indicating that some pattern remodeling continues even after sexual maturation (Figure 2—figure supplement 1B). As compared to xanthophores, erythrophores occur at lower densities and were more likely to be binucleated (Figure 2B, middle and right panels; Figure 2—figure supplement 1C and D), a characteristic associated with a mature state of differentiation in stripe melanophores of zebrafish (Saunders et al., 2019).

Because subtle differences in color can be difficult to discern, we sought metrics to describe mature and developing cells, under brightfield and fluorescent illumination in which these cells were distinguishable as well: xanthophores displayed green autofluorescence upon excitation with blue-green light (488 nm) owing to the presence of yellow carotenoids (Granneman et al., 2017; Saunders et al., 2019), whereas erythrophores showed only weak autofluorescence at this wavelength but much stronger red autofluorescence upon exposure to green-yellow light (561 nm) (Figure 2C). We then compared hue in brightfield illumination with relative red:green autofluorescence, confirming the differences between erythrophores and xanthophores (Figure 2D and E).

To understand the anatomical context of erythrophore development, we imaged fish during the larva-to-adult transformation. The first pigmented cells in the anal fin were lightly melanized melanophores. Subsequently, orange xanthophore-like cells appear that were pale and had smaller areas of visible pigment than mature erythrophores and xanthophores (Figure 2B, left panel; Figure 2—figure supplement 2). These early orange cells autofluoresced in both red and green channels, consistent with their appearance in brightfield (Figure 2F). During later development, however, cells in proximal regions were increasingly red whereas cells in distal regions were increasingly yellow. Cell densities gradually diverged between proximal and distal regions as well (Figure 2F; Figure 2—figure supplement 1D).

## Fin erythrophores and xanthophores arise from a common progenitor

As a first step in dissecting lineage relationships of erythrophores and xanthophores, we sought to determine whether these cells arise from a common early progenitor. Since red and yellow colors were likely carotenoid-based, we reasoned that lineage relationships should be revealed by clones of cells in fish mosaic for scavenger receptor *b1* (*scarb1*), which is essential for carotenoid accumulation in avian integument and zebrafish xanthophores (Toews et al., 2017; Toomey et al., 2017; Saunders et al., 2019). If erythrophores and xanthophores share a lineage, then rare wild-type clones should contain both red and yellow cells in an otherwise colorless background. If erythrophores and xanthophores have distinct lineage origins, however, wild-type clones should often contain only red cells or only yellow cells. In *D. albolineatus* injected with high efficiency AltR CRISPR/Cas9 reagents targeting *scarb1*, wild-type clones most often contained both red cells and yellow cells (Figure 3A).

We further assessed relationships by labeling individual clonal lineages by *tol2* transgenesis. We found that orange cells of larvae and both erythrophores and xanthophores of adults expressed transgenes driven by regulatory elements of *aldehyde oxidase 5* (*aox5*) isolated from zebrafish. *aox5* functions in the synthesis of pteridines present in xanthophores and erythrophores (see below) and is expressed by xanthophores and their specified precursors in zebrafish (Parichy et al., 2000; McMenamin et al., 2014). When we injected an *aox5* reporter transgene at limiting dilutions to express membrane-targeted EGFP, labeled cells were restricted to narrow regions along the anterior–posterior axis, consistent with derivation from single clones observed in other contexts (Tu and Johnson, 2010; Singh et al., 2014; Spiewak et al., 2018). Such cells occurred on the body and fin,

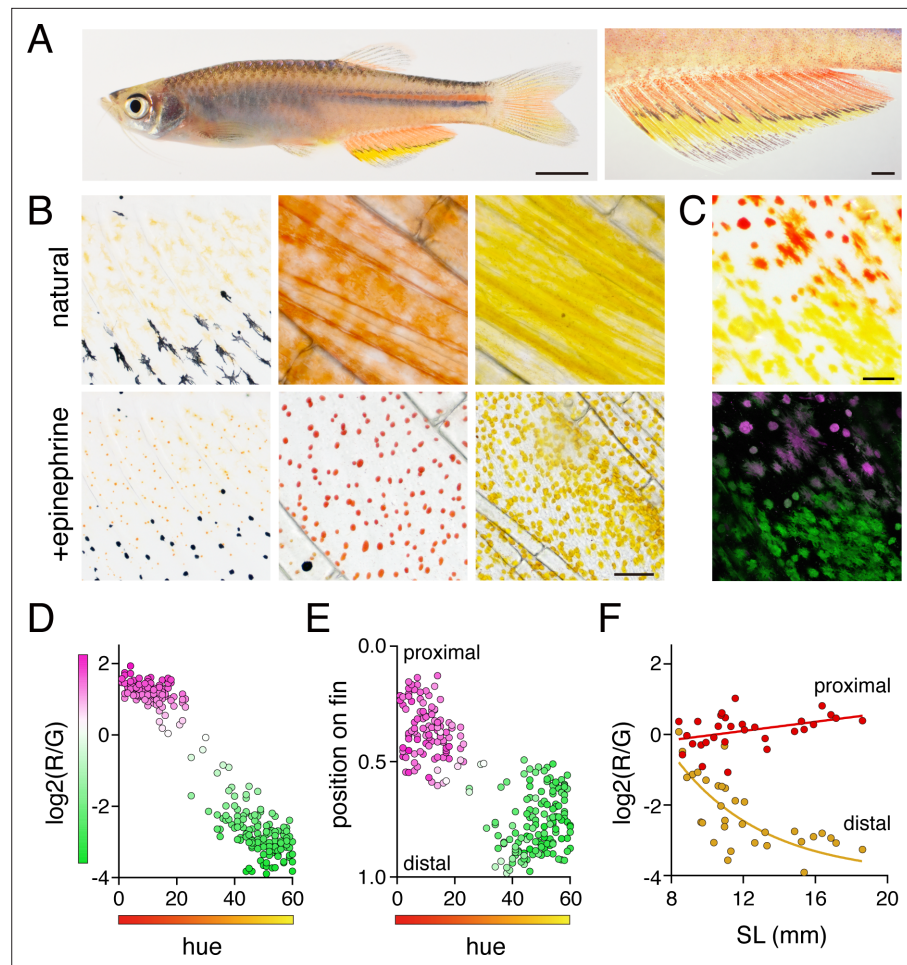


**Figure 2.** Anal fin pigment pattern of *D. albolineatus* and its ontogeny. **(A)** Erythrophares were present on the body and were particularly evident on the anal fin (closeup at right), where these cells were found more proximally than yellow xanthophores. **(B)** At larval stages xanthophore-like cells with a uniform orange coloration occurred across the entire fin (left panels). Later in the adult, proximal red erythrophares and distal yellow xanthophores have distinct colors (middle and right panels). **(C)** Erythrophares and xanthophores had different spectra under epifluorescence. Erythrophares autofluoresced in red (displayed in magenta) whereas xanthophores autofluoresced in green. **(D)** Hue values under brightfield illumination were correlated with ratios of red to green autofluorescence ( $R^2 = 0.92$ ,  $p < 0.0001$ ). **(E)** Colors of cells varied across the proximodistal axis of the fin, shown as relative position with fin base at 0 and fin tip at 1. Erythrophares in proximal regions were distinct in both fluorescence ratio and visible hue from xanthophores in distal regions though some intergradation was evident in middle regions, near the melanophore stripe.  $N = 250$  cells from five adult males in D and E. Color fills represent red to green fluorescence ratios. **(F)** During the larva-to-adult transformation, ratios of red to green autofluorescence diverged between prospective erythrophares and xanthophore regions. Individual red and yellow points correspond to mean values of cells in proximal and distal regions, respectively, from each of 31 male or female fish ( $N = 620$  cells total) imaged at a range of developmental stages represented by different standard lengths (SL). Scale bars: 5 mm (**A**, left), 1 mm (**A**, right); 25  $\mu\text{m}$  (**B**, **C**).

The online version of this article includes the following figure supplement(s) for figure 2:

**Figure supplement 1.** Sex and age differences in erythrophares pigmentation and occurrence of a binucleated state.

**Figure supplement 2.** Pattern development in anal fins of larva to juvenile fish.

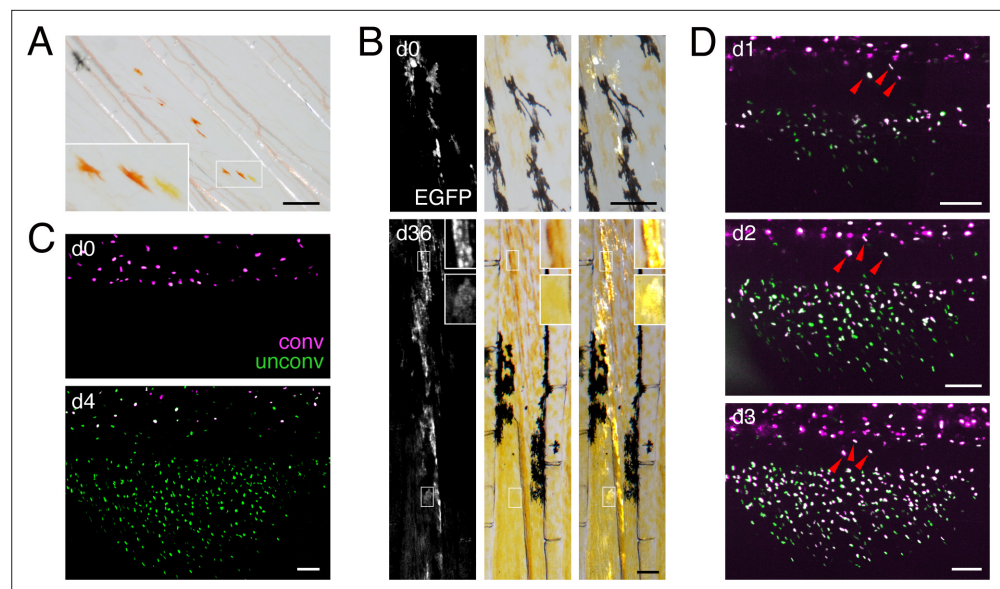


**Figure 3.** Shared progenitor of fin erythrophores and xanthophores revealed by clonal analyses. **(A)** In fish mosaic for somatically induced mutations in *scarb1* most rare, wild-type clones consisted of both erythrophores and xanthophores (8 of 10 presumptive clones in seven fish, with remaining clones only containing one or the other cell type; an additional 56 fish derived from injected embryos either lacked wild-type cells or lacked mutant cells and were thus uninformative). **(B)** Clonal labeling of xanthophores and erythrophores with *aox5:palmeGFP*, illustrating fluorescence, brightfield, and merged views of the same fields. In the clone shown here, an initial complement of several orange cells at the level of the melanophore stripe (d0, 7.5 mm SL) expanded to include more cells proximally and distally to the melanophore stripe that differentiated as erythrophores and xanthophores, respectively (d36, 15 mm SL; red arrowheads). For these analyses, limiting dilutions of *aox5:palmeGFP* were injected into ~500 embryos, yielding 271 embryos that exhibited some fluorescence at 3 days post-fertilization that were further sorted at 16 dpf, identifying 27 individuals with patches of expression in the anal fin. Of these 27 fish, one subsequently died and eight were found to have broad expression across the entire fin, likely representing multiple clones of uncertain boundaries, and so were excluded from analysis. The remaining 18 fish exhibited 24 spatially distinct, presumptive clones of *aox5:palmeGFP*-labeled cells, of which 22 presumptive clones contained both erythrophores and xanthophores as shown here [consistent with mixed clones of melanophores and xanthophores in zebrafish (Tu and Johnson, 2010; Tu and Johnson, 2011)]; one clone contained only erythrophores and one clone contained only xanthophores. **(C)** When *aox5:nucEosFP*<sup>+</sup> cells on the body were bulk photoconverted before fin development, only unconverted *aox5:nucEosFP*<sup>+</sup> cells (green nuclei) were present in the fin 4 days later (images representative of all N = 3 fish tested). **(D)** Successive steps in anal fin development and erythrophore/xanthophore lineage specification revealed many cells newly acquiring *aox5:nucEosFP* expression at daily intervals within the fin (green nuclei). Though some *aox5:nucEosFP*<sup>+</sup> cells were present at the fin base these did not enter into the fin proper (white cells, arrowheads; images shown are from a single individual representative of all N = 7 fish tested in this manner over 23 days each). Scale bars: 200  $\mu$ m (**A**, **B**); 100  $\mu$ m (**C**, **D**).

The online version of this article includes the following figure supplement(s) for figure 3:

**Figure supplement 1.** Transgene labeling of erythrophores and xanthophores.

and in these presumptive clones, erythrophores and xanthophores were almost always co-labeled (**Figure 3B**; **Figure 3—figure supplement 1**), consistent with a common progenitor for erythrophores and xanthophores.

A common progenitor could be specified for erythrophore or xanthophore fates either before or after colonizing the fin. To distinguish between these possibilities we used *aox5* reporter expression as an indicator of specification and a nuclear localizing photoconvertible (green→red) fluorophore, *nucEosFP*, to determine whether cells already expressing this marker transit from body to fin. We generated a transgenic line, Tg(*aox5:nucEosFP*)<sup>vp37albTg</sup>, which allowed us to photoconvert all *aox5:nucEosFP*<sup>+</sup> cells on the body prior to anal fin development (6.5 mm SL). We then assessed the distribution of converted and unconverted *nucEosFP* 4 days later, when the anal fin had started to form (7.5 mm SL). Because *aox5* expression persists once initiated, cells photoconverted at one stage will later have converted fluorophore (displayed in magenta), as well as new, unconverted fluorophore

(green), so nuclei will appear white; cells that initiate *aox5* expression only after photoconversion will have only unconverted fluorophore and nuclei that are green.

We found that cells on the body had converted and unconverted fluorophore, whereas cells in the fin had only unconverted fluorophore, consistent with initiation of *aox5* expression only after progenitors had colonized the fin (**Figure 3C**). Because it remained possible that some cells had migrated from body to fin and proliferated so extensively that signal of converted nucEosFP was lost by dilution, we repeated these analyses but assessed distributions of cells 1 d after photoconversion; we then photoconverted (or reconverted) all cells on body and fin and repeated this process on successive days. Such labeling failed to reveal cells that translocated from body to fin, although it did reveal numerous cells that acquired *aox5* expression when already in the fin (**Figure 3D**). Together these observations suggest that progenitors migrate to the fin, become specified for erythrophore or xanthophore lineages within the fin, and then contribute to both populations as they proliferate to populate the proximal–distal axis during fin outgrowth.

### **Erythrophores and xanthophores arise from fate-restricted and unrestricted precursors in the fin and their fates remain plastic even after differentiation**

Clones identified by *scarb1* activity or *aox5* transgene expression (**Figure 3A and B**) likely represented progenitors segregated from other lineages during early development when injected Cas9 is active and transgene integration occurs (e.g., *Tryon et al., 2011*); these clones presumably also included melanophores or other cell types not revealed by these markers (*Tu and Johnson, 2010; Tu and Johnson, 2011; Lewis et al., 2019*). We therefore asked whether progeny of such clones that had already colonized the fin were restricted to either erythrophore or xanthophore fates by photoconverting individual nucEosFP+ cells at early stages of fin development (7.0–8.5 mm SL) and then assessing phenotypes of resulting clones 30–36 days later (15.0 mm SL). At 7.0 mm SL, only unpigmented nucEosFP+ cells were present (**Figure 4A, top**). Preliminary observations indicated that proximally located cells tended to remain in the proximal region where erythrophores develop, so we photoconverted cells in distal regions that might become more broadly distributed. Resulting clones consisted of erythrophores if daughter cells remained relatively proximal as the fin grew out, or both erythrophores and xanthophores if daughter cells became distributed across the proximodistal axis (**Figure 4B and C; Figure 4—figure supplement 1A**). At 7.5 mm, many nucEosFP+ cells had acquired a pale orange color (**Figure 4A, bottom**) and so we asked whether these cells had become fate-restricted with the onset of pigmentation. Similar to unpigmented cells, however, initially proximal orange cells generated only erythrophores, whereas initially distal orange cells could generate clones of only erythrophores, both erythrophores and xanthophores, or only xanthophores, depending on where daughter cells were distributed (**Figure 4C; Figure 4—figure supplement 1B**). Finally, at 8.5 mm we found that still-unpigmented nucEosFP+ cells near the distal fin tip generated distal clones restricted to a xanthophore fate (**Figure 4—figure supplement 1C**). These results show that individual unpigmented cells and early-developing orange cells in the fin can generate both erythrophores and xanthophores, depending on initial location and where progeny localize.

We further asked whether phenotypes of erythrophores and xanthophores might be plastic even after they differentiate by challenging cells in a regenerative context. To test for erythrophore → xanthophore conversion, we amputated fins through the region containing erythrophores, expecting that regeneration distally might allow for repositioning of erythrophores into regions where regenerative xanthophores would be expected, with conditions favorable to fate conversion, should cells retain such potential. We first assessed the possibility that transfating occurs by repeatedly imaging individual fish in brightfield, to learn whether cells near the amputation plane might lose their red color during regenerate outgrowth. Individual erythrophores could often be reidentified using other cells as well as distinctive features of fin ray bones and joints as landmarks (**Figure 5A; Figure 5—figure supplement 1**). As regeneration proceeded, small groups of cells having paler red or orange coloration, were sometimes observable where individual cells of deep red coloration had been found, suggestive of proliferation and dilution of pre-existing pigments. Later, only yellow cells were found in these same locations. These observations were consistent with the possibility of erythrophore → xanthophore conversion. To test this idea directly we marked nucEosFP+ erythrophores by photoconversion prior to amputation and followed labeled cells through regeneration (**Figure 5B; Figure 5—figure**

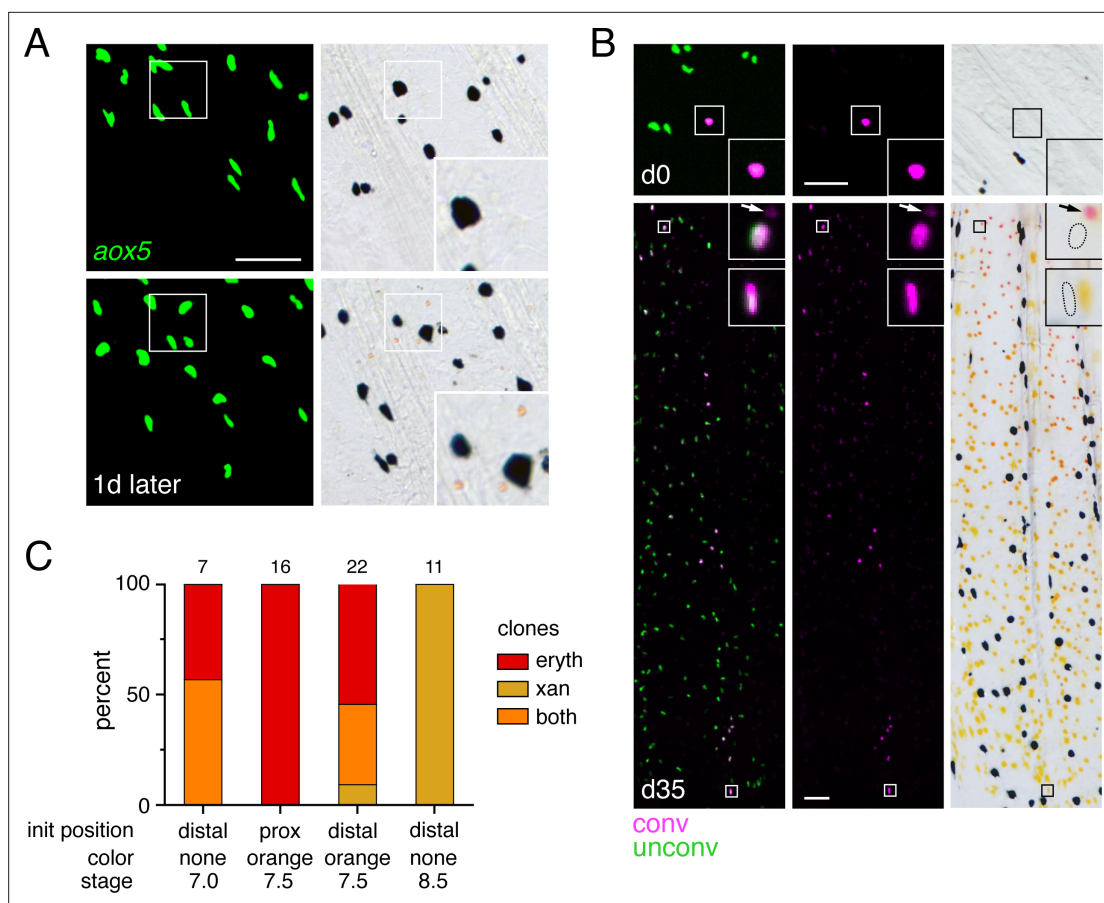


**Figure 4.** Bipotential precursor to erythrophores and xanthophores revealed in the fin by fate mapping. **(A)** Unpigmented cells of the xanthophore lineage, marked by *aox5:nucEosFP* transgene expression (see Main text), present at 7.0 mm SL had acquired a pale orange color 1 day later. (Representative of all N = 7 fish examined by repeated imaging during larval development.) Insets show higher magnification images of a corresponding region. **(B)** Example of a photoconverted, initially unpigmented cell (d0, 7.0 mm SL) that yielded a clone containing both erythrophores and xanthophores (d35, 15.0 mm SL; representative of four of seven clones, with remaining clones containing erythrophores only). Fish were treated with epinephrine to contract pigment before imaging. Arrows indicate erythrophore autofluorescence from red carotenoid pigment, which accumulates adjacent to nuclei following epinephrine treatment; approximate positions of *nucEosFP*+ nuclei in brightfield images are shown with dashed outlines. Insets, proximal and distal cells in the clone. **(C)** Percentages of clones containing only erythrophores, only xanthophores, or both cell types. Numbers above bars indicate clone sample sizes examined. In these analyses pigment cells and progenitors stably expressed *aox5:nucEosFP* (7.5, 8.5 mm SL) or mosaically expressed a different transgene, *mitfa:nucEosFP* (7.0 mm SL), that had been injected into embryos at the one-cell stage. In zebrafish, *mitfa* (*melanophore-inducing transcription factor a*) is expressed by pigment cell progenitors, as well as melanophores and xanthophores (Lister et al., 1999; Budi et al., 2011; Saunders et al., 2019), and we found in *D. albolineatus* that *mitfa:nucEosFP* was expressed in these cells as well as orange cells of larvae and erythrophores of adults. *mitfa:nucEosFP* was used for fate mapping at early stages owing to its more robust expression in unpigmented cells. Scale bar: 50  $\mu$ m.

The online version of this article includes the following figure supplement(s) for figure 4:

**Figure supplement 1.** Fate mapping of single photoconverted cells at different locations and stages.

**supplement 2A).** Many erythrophores divided to replenish their complement in proximally regenerating tissue, and a few erythrophores differentiated from unpigmented precursors, as indicated by the presence, or absence of photoconverted *nucEosFP*, respectively (Figure 5—figure supplement 2B). Additionally, some initially marked erythrophores came to occupy more distal regions and were indistinguishable from regenerative xanthophores that had developed from unpigmented progenitors even 36–51 days post-amputation (Figure 5C). These findings suggest a reduction in pre-existing red pigment as cells divide, and a failure to accumulate new red pigments once proliferation has ceased. We also sought to determine whether xanthophores can transition to an erythrophore fate by ablating central regions of fin and then assessing whether distal xanthophores can move into the regenerating proximal region. However, these experiments were not informative, as regenerative tissue was



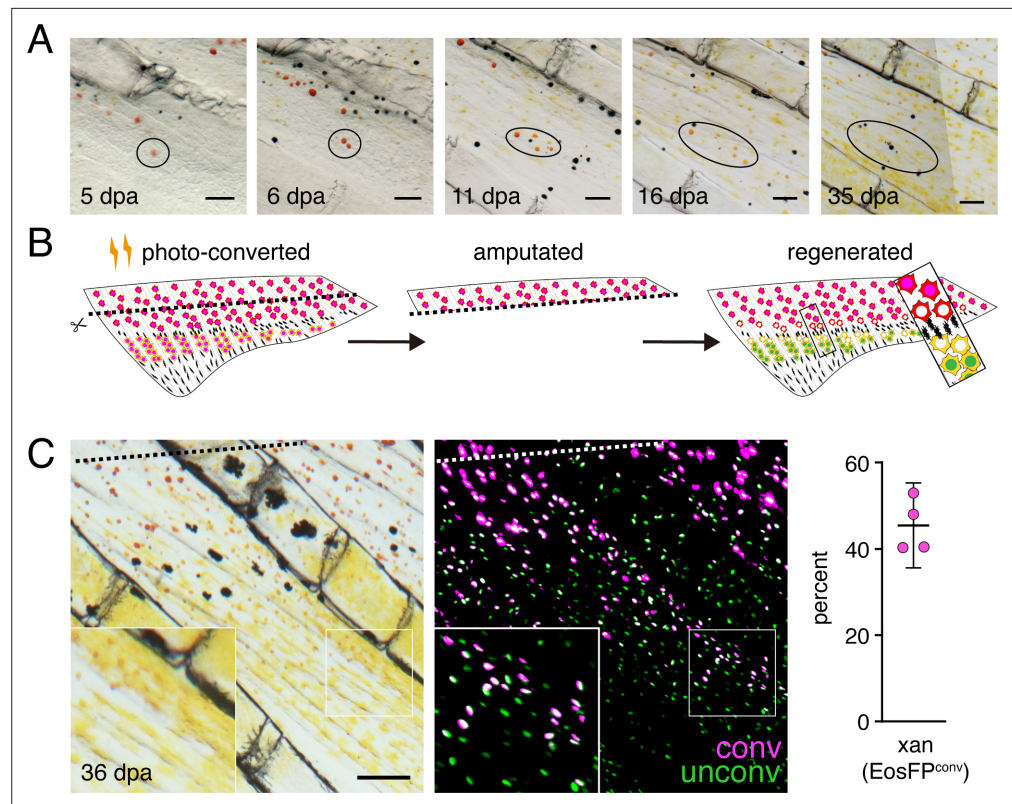


**Figure 5.** Regeneration assays reveal fate plasticity in differentiated cells and latent stem cells competent to differentiate as erythrophores and xanthophores. **(A)** Brightfield sequence of regeneration illustrating apparent conversion of erythrophores to xanthophores (image series representative of all  $N = 3$  fish examined by repeated imaging through regeneration). As fins regenerated, individual erythrophores (circled) near the amputation plane appeared to divide, with presumptive daughter cells having reduced amounts of pigment visible upon contraction with epinephrine and an increasingly yellow–orange color. **(B)** Schematic of regeneration experiment in C. Fins of *Tg(aox5:nucEosFP)* fish were photo-converted *in toto* prior to amputation through the erythrophore region. Fins regenerated over 15 days and pigment pattern had re-formed by 30 days, at which time a new melanophore stripe and distinct regions of erythrophores and xanthophores had developed. **(C)** Example of cells in regenerative tissue 36 days post-amputation (dpa). Regenerative xanthophores near the plane of amputation often contained photoconverted *nucEosFP* in a region of fin extending 400  $\mu\text{m}$  from the distalmost red erythrophore into the regenerative xanthophore region (means  $\pm$  95 % confidence interval;  $N = 1964$  cells in four fish examined). Dashed lines indicate amputation in B and C. Scale bars: 50  $\mu\text{m}$  (A); 100  $\mu\text{m}$  (C).

The online version of this article includes the following figure supplement(s) for figure 5:

**Figure supplement 1.** Pigment cell arrangements and colors and fin tissue context during pattern regeneration.

**Figure supplement 2.** Regeneration of erythrophores from newly specified unpigmented progenitors.

**Figure supplement 3.** Regeneration of central fin regions.

colonized by erythrophores or xanthophores differentiated from progenitors rather than pre-existing xanthophores (**Figure 5—figure supplement 3**).

These observations indicate that erythrophores and xanthophores of the adult anal fin share a lineage, that individual progenitor cells within the fin can contribute to both cell types, and that some plasticity in fate persists even after differentiation, with erythrophores able to transition to a yellow-pigmented phenotype when challenged to do so.

### Genetic requirements and biochemical basis for red coloration

To better understand molecular mechanisms of red coloration we compared gene expression between fin regions containing only erythrophores or only xanthophores. Erythrophores occurred at only ~one-third the density of xanthophores in two dimensional images (**Figure 2—figure supplement 1D** and see below) and proximal and distal fin regions presumably differ in ways other than chromatophore

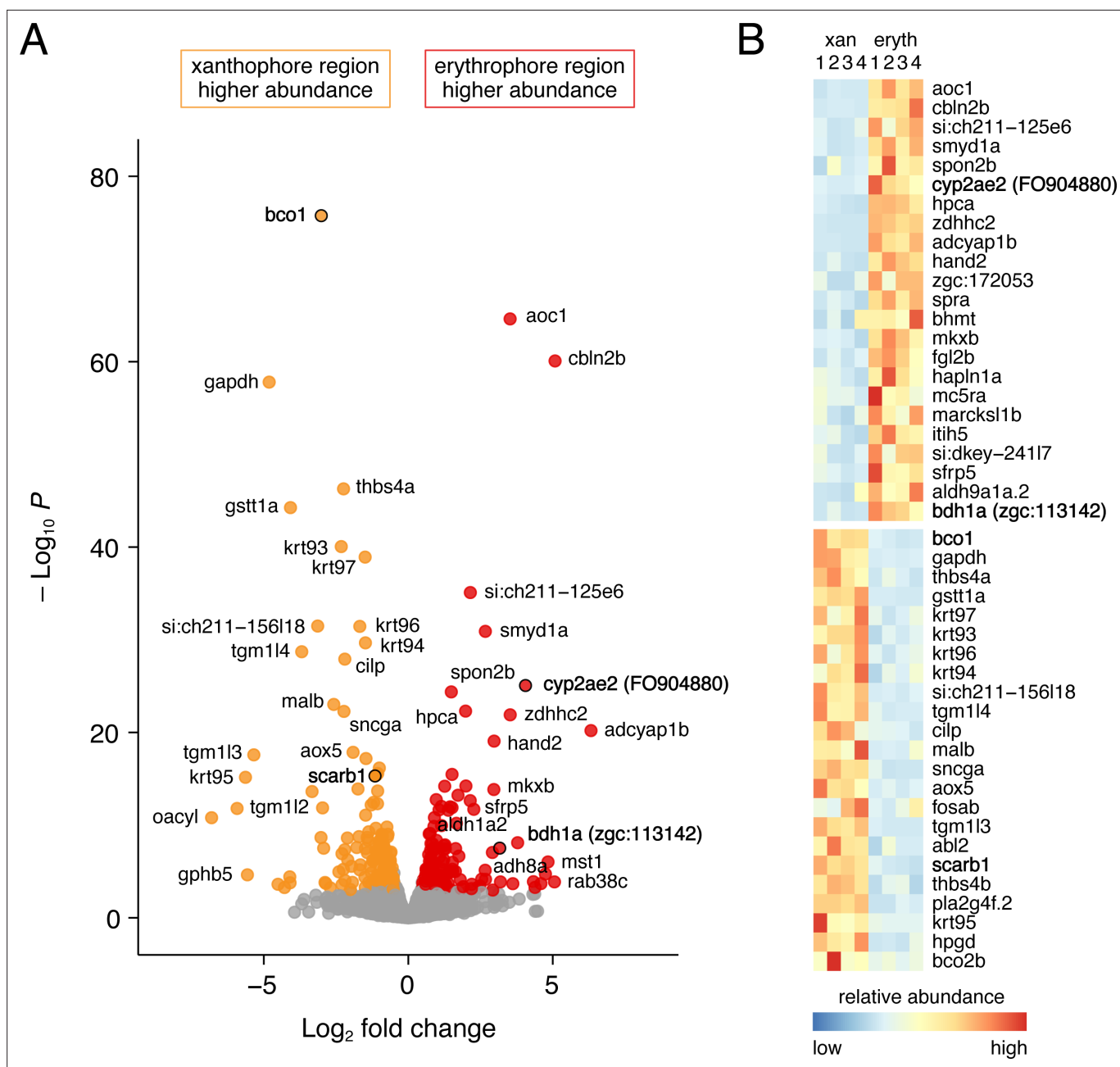


**Figure 6.** Differential gene expression in fin regions with erythrohores and xanthophores. **(A)** Volcano plot of detected transcripts. Yellow–orange and red points indicate transcripts more abundant in xanthophore-containing and erythrofore-containing regions, respectively ( $q \leq 0.05$ ). Gray points, transcripts not significantly different in abundance between regions. **(B)** Heat maps illustrating differential expression of selected loci across fin regions and replicate libraries. Genes with names in bold had phenotypes affecting erythrofore pigmentation.

content. Nevertheless, we reasoned that comparisons of bulk tissue preparations might still identify genes having marked differences in expression between erythrohores and xanthophores, as would be expected for loci functioning in pigment synthesis (Saunders *et al.*, 2019). Mapping *D. albolineatus* sequencing reads to the zebrafish genome identified 18,050 expressed genes. Transcripts of 162 genes were more abundant in proximal erythrofore-containing tissue, whereas transcripts of 200 genes were more abundant in distal xanthophore-containing tissue ( $q < 0.05$ ; fold-changes = 0.4–6.8) (Figure 6A and B; Supplementary file 1—Table 1).

To identify genes required for red or yellow coloration, we used CRISPR/Cas9 mutagenesis to knock out selected candidates that might have roles in processing of carotenoids, synthesis of other

pigments, or fate specification (**Supplementary file 1**—Tables 2 and 3). We screened mosaic (F0) fish and isolated stable lines of mutant alleles for target genes with pigmentary phenotypes. Of 25 targets derived from RNA-seq, three yielded mutants with defects in pigmentation. To determine which pigments contributed to colors present in wild-type, and which were affected in mutants, we further assayed the carotenoid content of fin regions by HPLC.

In the wild type, fin tissue containing erythrohores was markedly enriched for the red ketocarotenoid astaxanthin; additional peaks had profiles consistent with other ketocarotenoids (**Figure 7A**, peak 3; **Figure 7—figure supplement 1**; **Supplementary file 1**—Table 4). Fin tissue containing xanthophores lacked astaxanthin and instead contained yellow zeaxanthin (peak 10), similar to zebrafish xanthophores (**Saunders et al., 2019**), as well as additional peaks characteristic of other yellow xanthophyll carotenoids.

To confirm that carotenoids rather than other pigments are principally responsible for pigmentation, we recovered mutant alleles of *scarb1*, required for carotenoid uptake and localization (**Toomey et al., 2017**; **Saunders et al., 2019**), as residual color in such mutants would suggest a non-carotenoid contribution. We isolated two alleles, *scarb1*<sup>vp38ac1</sup> (V84Δ16X) and *scarb1*<sup>vp38ac2</sup> (V84X), and found that *scarb1*<sup>vp38ac1/vp38ac2</sup> individuals had a phenotype concordant with that of F0 mosaics (**Figure 3A**): they lacked color in the visible range and lacked carotenoids detectable by HPLC (**Figure 7B**; **Figure 7—figure supplement 2A**; **Supplementary file 1**—Table 4). The absence of residual red or yellow coloration suggested that pteridine pigments do not contribute to visible color in these cells, as they do in some other species (**Goodrich et al., 1941**; **Matsumoto and Obika, 1968**; **Grether et al., 2001**; **Weiss et al., 2012**; **Olsson et al., 2013**). Moreover, targeting of differentially expressed genes known to function in pteridine synthesis did not yield visible pigmentation defects in F0 mosaics (erythrofore region: *spra*, *xdh*; xanthophore region: *aox5*; **Supplementary file 1**—Tables 1 and 4). Pteridine pigments were detectable histologically in erythrohores and xanthophores, however, and could be visible to fish in the UV range (**Figure 7—figure supplement 2B**).

Mutants for two genes, *cyp2ae2* (FO904880.1) and *bdh1a* (*zgc:113142*), lacked overt red coloration (**Figure 7C**; **Figure 7—figure supplement 2A**), although densities of erythrohores and xanthophores did not differ significantly from wild-type (**Figure 7F**). Both genes had transcripts that were more abundant in fin tissue containing erythrohores than xanthophores ( $\log_2$  fold-changes = 4.9, 2.1;  $q = 9.6E-23$ ,  $8.9E-8$ ; **Figure 6**). We confirmed by RT-PCR that both genes were expressed in erythrohores picked manually by micropipette from dissociated fin tissue (**Figure 7—figure supplement 3A**).

*cyp2ae2* encodes an enzyme within the large family of cytochrome P450 monooxygenases (**Kirschian et al., 2011**). A related gene encoding a different P450 family member, *CYP2J19*, is essential for red coloration in ‘red factor’ canary (**Lopes et al., 2016**) and zebra finch (**Mundy et al., 2016**), and likely has similar roles in other birds and turtles (**Twyman et al., 2016**; **Twyman et al., 2018**). *CYP2J19* expression is testosterone-dependent (**Khalil et al., 2020**) and its product is believed to play an essential role in the conversion of yellow carotenoids like zeaxanthin into red ketocarotenoids like astaxanthin (**Figure 1A**). Orthologs of *CYP2J19* appear to be restricted to birds and turtles (**Twyman et al., 2016**). Reciprocally, *cyp2ae2* (FO904880.1) is clearly a member of the *cyp2* family, and is likely orthologous to *cyp2ae1* loci of other teleosts by sequence similarity and chromosomal position, yet no clear orthologues of this gene are present in amniotes (Ensembl Release 103) (**Kirschian et al., 2011**; **Yates et al., 2020**). The loss of red color in *D. albolineatus* erythrohores thus raises the possibility that *CYP2J19* and *Cyp2ae2* may have acquired carotenoid ketolase activity convergently. Supporting the idea that *cyp2ae2* might encode a carotenoid ketolase, the *cyp2ae2* mutant had markedly reduced amounts of astaxanthin in fin regions containing erythrohores but relatively greater amounts of zeaxanthin (peak 10) in both erythrofore and xanthophore containing tissue as compared to wild-type, consistent with *cyp2ae2* expression in both tissues, albeit at different levels (**Figure 7—figure supplement 1**, **Supplementary file 1**—Table 5). Consistent with these findings, erythrohores of *cyp2ae2* mutants had markedly reduced red/green fluorescence ratios (**Figure 7D**) and a reduced diameter of visible pigment (**Figure 7E**). Trace residual astaxanthin and other ketocarotenoids are unlikely to reflect residual activity of *cyp2ae2*, as the mutant allele, *cyp2ae2*<sup>vp39ac1</sup>, harbors a five-nucleotide frameshift within the first coding exon leading to 42 novel amino acids followed by a premature stop codon (L46Δ43X). A paralogous locus, *cyp2ae1*, lies adjacent to *cyp2ae2* and was expressed at very low levels in both fin regions (**Figure 7—figure supplement 3B**; **Supplementary**

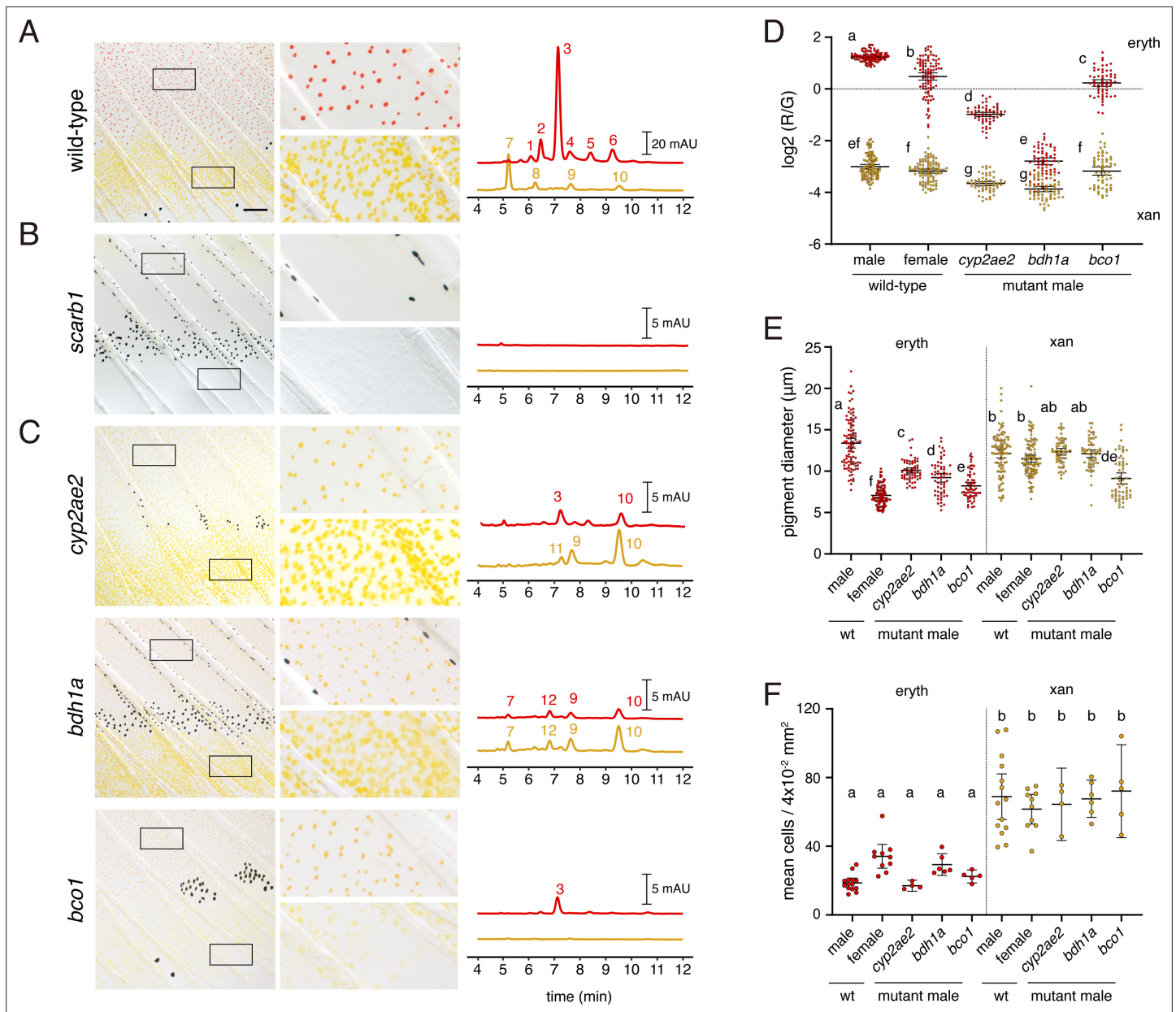


**Figure 7.** Wild-type pigment composition and mutant phenotypes. **(A)** Wild-type fin and carotenoid profile, showing carotenoid absorbance at 455 nm in adult male proximal tissue (red) and distal tissue (yellow). Numbers indicate different carotenoid species, with the most abundant ketocarotenoid in erythrofore-containing tissue being astaxanthin (peak 3; **Figure 1A**; **Figure 7—figure supplement 1**). **(B)** Homozygous *scarb1* mutants lacked red and yellow coloration and carotenoids were not detectable. **(C)** Homozygous mutant phenotypes of genes targeted from RNA-Seq comparisons. *cyp2ae2* and *bdh1a* mutants were deficient for red color and astaxanthin. *bco1* mutants had reduced red and yellow coloration and carotenoids. **(D)** Ratios of red to green autofluorescence for cells found within proximal erythrofore containing regions (red filled points) and distal xanthophore containing regions (yellow filled points) of wild-type males and females compared to mutant males. In the wild-type, erythrofores and xanthophores were segregated into different populations by R/G fluorescence, although differences in females were less marked. In males of each mutant, R/G ratios of erythrofores were reduced compared to wild-type, and lesser reductions were evident in xanthophores (ANOVA, genotype x region interaction,  $F_{4,736}=310.82$ ,  $p < 0.0001$ , after controlling for significant main effects and variation among individuals;  $N = 760$  cells total from five individuals of each background). Plots show means  $\pm$  95 % confidence intervals; means of groups not sharing the same letter differed significantly from one another ( $p < 0.05$ ) in Tukey-Kramer *post hoc* comparisons. **(E)** Wild-type males and females, and mutant males, differed in total visible pigment, as measured by diameters of contracted pigment granules following epinephrine treatment (**Saunders et al., 2019**). (ANOVA, background x region interaction,  $F_{4,736}=76.25$ ,  $p < 0.0001$ , with significant main effects and variation among individuals; diameters were *ln*-transformed for analysis to control for increasing residual variance with means.). **(F)** Densities of erythrofores and xanthophores differed across backgrounds (ANOVA, background x region interaction,  $F_{1,35}=19.01$ ,  $p < 0.0001$ ). Each point represents the mean number of cells counted in three regions of  $4 \times 10^{-2}$  mm<sup>2</sup> in proximal or distal regions with erythrofores or

Figure 7 continued on next page

Figure 7 continued

xanthophores, respectively, in each of 39 total fish. Scale bar: 50  $\mu$ m.

The online version of this article includes the following figure supplement(s) for figure 7:

**Figure supplement 1.** Characteristics of carotenoid absorbance spectra.

**Figure supplement 2.** Mutant lesions recovered, presence of pteridines, and mosaic phenotype of *bco1*.

**Figure supplement 3.** Expression, genomic location and additional phenotypes of genes contributing to red coloration.

**file 1—Table 1).** Compensatory activity of *cyp2ae1* might account for trace levels of ketocarotenoids in *cyp2ae2<sup>vp39ac1</sup>*.

The second red-deficient mutant, *bdh1a*, encodes 3-hydroxybutyrate dehydrogenase type 1a, a short-chain dehydrogenase/reductase. Homologues of this gene in mammals are known to interconvert hydroxyl and ketone groups, and in particular acetoacetate and 3-hydroxybutyrate, two major ketone bodies (Green et al., 1996; Langston et al., 1996; Persson et al., 2009; Otsuka et al., 2020). Although not implicated previously in carotenoid processing or red coloration, transcripts of a homologous gene were enriched in orange skin of clownfish *Amphiprion ocellaris* (Salis et al., 2019). The *bdh1a<sup>vp40ac1</sup>* mutant (D141 $\Delta$ 12X) completely lacked astaxanthin and other ketocarotenoids in erythrophore-containing tissue, and did not exhibit increased levels of zeaxanthin, as observed in *cyp2ae2<sup>vp39ac1</sup>* (Figure 7C). Red/green fluorescence ratios of erythrophores are similar to those of xanthophores (Figure 7D) and the diameter of visible pigment is reduced from wild-type levels in erythrophores though not xanthophores (Figure 7E), confirming the visible phenotype.

Erythrophores of *cyp2ae2* and *bdh1a* mutant fish appeared normal in size and shape in young adults yet became morphologically heterogeneous as fish age, with pigment-containing cell fragments and fewer cells evident, as well as an onset of whole-fish kyphosis by ~12 months post-fertilization (Figure 7—figure supplement 3C). These phenotypes suggest requirements for both loci in the accumulation of red carotenoids and subsequent homeostasis of erythrophores and other tissues, perhaps associated with a systemic dysregulation of carotenoid–Vitamin A–retinoid metabolism (von Lintig et al., 2005; Ghyselinck and Duester, 2019).

$\beta$ -carotene oxygenase 1 (Bco1) symmetrically cleaves  $\beta$ -carotene to produce vitamin A, a precursor of retinoic acid; whereas  $\beta$ -carotene oxygenase 2 (Bco2) cleaves a variety of carotenoids in an asymmetric fashion, often leading to their degradation (Widjaja-Adhi et al., 2015; Li et al., 2017; Harrison and Kopeck, 2020; Poliakov et al., 2020). *bco1* and *bco2b* were more abundant in tissue containing xanthophores than erythrophores ( $\log_2$ FC = 4.9, 2.1;  $q$  = 9.6E-23, 8.9E-8); a third locus, *bco2l* was similarly abundant at both sites (Supplementary file 1—Table 1). Given heterogeneities in transcript abundance, we asked whether  $\beta$ -carotene oxygenase genes might also contribute to differences in carotenoid accumulation between cell types. Only *bco1*-targeted fish exhibited an overt pigmentary phenotype in F0 mosaic animals, with pigment-free patches alongside patches of cells having apparently normal pigmentation consistent with a pigment-cell autonomous function (Figure 7—figure supplement 2C). Mutants stably carrying *bco1* alleles (*bco1<sup>vp41ac1</sup>*, 52D $\Delta$ 5X; *bco1<sup>vp41ac2</sup>*, 51F $\Delta$ 9X) had reduced carotenoid levels in both xanthophores and erythrophores as well as smaller diameters of contracted pigment granules (Figure 7C–E; Figure 7—figure supplement 2A and B). The mechanism of this effect on chromatophore carotenoid content remains unclear.

## Discussion

Red and orange coloration play important roles in multiple behaviors, including mate choice (see Introduction). As a first step toward understanding the development of such colors and the mechanisms underlying their phylogenetic distribution in the zebrafish genus *Danio*, we investigated the cell lineage origins and genetic requirements for erythrophore differentiation in *D. albolineatus*. These analyses provide new insights into the diversification of adult pigment cell types in teleosts and identify genes contributing to the red ketocarotenoid coloration in this species and possibly more distant taxa as well.

Fate mapping and clonal analyses indicated that at least some erythrophores and xanthophores share a common progenitor in the fin. Clones of cells marked genetically during early development later contained both cell types, indicating a shared progenitor that likely colonizes the fin during

its initial outgrowth, consistent with inferences for melanophore and xanthophore progenitors of zebrafish fins (Tu and Johnson, 2010; Tu and Johnson, 2011). In *D. albolineatus*, these progenitors appear to become specified for erythrophore or xanthophore fates—as inferred from *aox5* transgene expression—only after colonizing the fin. We did not observe pigmented cells transit from the body to the fin, though such cells could be found at the base of the fin without entering the fin itself. These findings might appear to differ from that of a prior study, in which erythrophores on the body were described as invading the fin (Goodrich and Greene, 1959). Yet those observations were made with the caveat that an appearance of invasion could also reflect de novo differentiation within regions not previously occupied by these cells, rather than active migration per se. We conclude that unpigmented progenitors enter the fin and only then become specified to erythrophore or xanthophore fates.

At early stages of fin outgrowth, some initially unpigmented progenitors acquire an orange color, intermediate between that of fully differentiated erythrophores and xanthophores. When these early orange cells were marked individually by photoconversion of a transgenic reporter, some cells initially at middle positions along the fin proximodistal axis gave rise to both erythrophores and xanthophores, whereas other more proximal or more distal cells contributed to only erythrophore or xanthophores, respectively. These observations indicate a bipotentiality, with fate choice presumably dependent on factors in the fin environment. Our finding that erythrophores can lose their red color when joining a regenerative population of xanthophores further indicates a subsequent plasticity in these fates. At later stages of fin development, unpigmented cells developed directly as xanthophores in distal regions. Whether these represent a distinct sublineage remains to be determined.

Red and orange colors can be generated in various ways. In mammals, reddish hues typically depend on the production of phaeomelanin by melanocytes, which is transferred to keratinocytes for incorporation into hair (Slominski et al., 2005; Hubbard et al., 2010; Tadokoro and Takahashi, 2017; Caro and Mallarino, 2020). In birds, phaeomelanin is also known to contribute to brownish-red feather coloration (McGraw et al., 2005; Cruz-Miralles et al., 2020), but more vibrant reds and oranges typically depend on carotenoids, accumulated, processed, and eventually deposited in developing feathers (Lopes et al., 2016; Mundy et al., 2016; Toews et al., 2017). In lizards, reds are most often the result of pteridine pigments (Olsson et al., 2013), contained within xanthophores, whereas in amphibians and teleosts these colors can result from pteridines as well as carotenoids in xanthophores and erythrophores (Matsumoto, 1965; Wedekind et al., 1998; Grether et al., 2001; Bagnara and Matsumoto, 2006; Sefc et al., 2014). Our analyses show that in *D. albolineatus*, red and orange colors of adult erythrophores and xanthophores result from carotenoids, detectable by HPLC and lost in *scarb1* mutants. Though pteridines were detectable histologically in erythrophores these did not affect color in the visible range. These observations are concordant with findings from zebrafish, in which the yellow–orange color of xanthophores in adults depends on carotenoids (Saunders et al., 2019), whereas yellow coloration of the same cells in embryos and early larvae depends on pteridines (Ziegler, 2003; Lister, 2019).

The precise biochemical mechanism whereby yellow carotenoids (e.g., zeaxanthin) are converted into ketocarotenoids in animals remains incompletely understood (Strange, 2016; Toews et al., 2017). In birds, an essential role has been demonstrated for CYP2J19, which is thought to mediate the C4-ketolation of carotenoids (Lopes et al., 2016; Mundy et al., 2016). Our analyses show that another member of the *cyp2* P450 subfamily, *cyp2ae2*, is important for ketocarotenoid accumulation in erythrophores. The finding that two different members of the *cyp2* subfamily may have converged on a role in ketocarotenoid formation, suggests that this subgroup of P450 enzymes may be uniquely poised to evolve ketolase activity. Nevertheless, the biochemical function of these enzymes has yet to be demonstrated in vitro, and full ketolase activity may depend on additional factors. In this regard, the markedly reduced abundance of red carotenoids in *bdh1a* mutant erythrophores may provide further clues to the biochemical mechanism of ketocarotenoid production. Indeed, our finding that *bco1* mutants have reduced levels of both red and yellow carotenoids—contrary to the expected activity of this enzyme in carotenoid degradation (Harrison and Kopec, 2020) and observations in other systems—suggests biochemical functions and compensatory interactions in this system worthy of further exploration.

The diversification of pigment patterns in teleost has been accompanied by a diversification of pigment cell types, with several distinct classes of iridophores, xanthophores, and leucophores now

recognized in *Danio* fishes alone (Oshima and Kasai, 2002; Hirata et al., 2003; Lewis et al., 2019; Saunders et al., 2019; Gur et al., 2020). Additional subtypes of pigment cells and even mosaic pigment cells with properties of more than one type have been recognized in more distant teleosts (Ballowitz, 1913; Goodrich et al., 1941; Asada, 1978; Goda and Fujii, 1995; Goda et al., 2011; Goda et al., 2013; Djurdjević et al., 2015; Salis et al., 2019; Parichy, 2021). In at least one instance cells of one type can transition directly into another type (melanophores→ melanoleucophores) (Lewis et al., 2019), whereas in another instance subtypes derived from a common progenitor (stripe and interstripe iridophores) are refractory to interconversion even when challenged to do so experimentally (Gur et al., 2020). Our observations of erythrophore and xanthophore origins and fate plasticity suggest a relatively subtle distinction, perhaps limited to the activation or repression of genes essential for the color difference itself. The particular mechanisms that specify these fates or deployment of particular biochemical pathways, and whether additional phenotypes distinguish these cells remain to be elucidated. Such efforts in *D. albolineatus*, and corresponding investigations to uncover genetic bases of erythrophore loss in zebrafish, will be enabled by the identification of cell-type-specific pigments and the development of methods to quantify pigmentary phenotypes in live animals.

## Materials and methods

### Key resources table

Reagent type (species or resource)*	Designation	Source or reference	Identifiers	Additional information
Genetic reagent ( <i>D. albolineatus</i> )	Tg( <i>aox5:nucEos</i> ) <sup>vp37albTg</sup>	This paper		Transgenic line. Maintained in Parichy lab. Described in Materials and methods.
Genetic reagent ( <i>D. albolineatus</i> )	<i>scarb1</i> <sup>vp38ac1</sup>	This paper		CRISPR-CAS9 knock-out line. Maintained in Parichy lab. Described in Materials and methods, and <b>Figure 7—figure supplement 1</b> .
Genetic reagent ( <i>D. albolineatus</i> )	<i>scarb1</i> <sup>vp38ac2</sup>	This paper		CRISPR-CAS9 knock-out line. Maintained in Parichy lab. Described in Materials and methods, and <b>Figure 7—figure supplement 1</b> .
Genetic reagent ( <i>D. albolineatus</i> )	<i>cyp2ae2</i> <sup>vp39ac1</sup>	This paper		CRISPR-CAS9 knock-out line. Maintained in Parichy lab. Described in Materials and methods, and <b>Figure 7—figure supplement 1</b> .
Genetic reagent ( <i>D. albolineatus</i> )	<i>bdh1a</i> <sup>vp40ac1</sup>	This paper		CRISPR-CAS9 knock-out line. Maintained in Parichy lab. Described in Materials and methods, and <b>Figure 7—figure supplement 1</b> .
Genetic reagent ( <i>D. albolineatus</i> )	<i>bco1</i> <sup>vp41ac1</sup>	This paper		CRISPR-CAS9 knock-out line. Maintained in Parichy lab. Described in Materials and methods, and <b>Figure 7—figure supplement 1</b> .
Genetic reagent ( <i>D. albolineatus</i> )	<i>bco1</i> <sup>vp41ac2</sup>	This paper		CRISPR-CAS9 knock-out line. Maintained in Parichy lab. Described in Materials and methods, and <b>Figure 7—figure supplement 1</b> .
Recombinant DNA reagent	<i>mitfa:nucEosFP</i>	This paper		Maintained in Parichy lab. Described in Materials and methods.
Recombinant DNA reagent	<i>aox5:palmEGFP</i>	<b>McMenamin et al., 2014</b>		
Software, algorithm	JMP Pro 16	SAS Institute		
Software, algorithm	GraphPad Prism	GraphPad		
Software, algorithm	Fiji	<b>Schindelin et al., 2012</b>		
Software, algorithm	Kallisto	<b>Bray et al., 2016</b>		
Software, algorithm	DESeq2	<b>Love et al., 2014</b>		

\* Additional oligonucleotides and CRISPR/Cas9 reagents provided in **Supplementary file 1—Table 2 and 5**.

## Fish stocks and rearing conditions

*Danio albolineatus* were derived from individuals collected in Thailand by M. McClure in 1995 (McClure et al., 2006), provided to the laboratory of S. Johnson, and then maintained in our laboratory from 2000 until the present. Additional species of *Danio* used for assessing erythrocyte complements were obtained directly from the field or through the pet trade [*D. aesculapii*; *D. quagga*, *D. kyathit* (McCluskey et al., 2021) *D. nigrofasciatus*, *D. tinwini* (Spiewak et al., 2018); *D. kerri*; *D. choprae*; *D. margaritatus*, *D. eythromicron*] and maintained subsequently in the lab or were observed in the field [*D. meghalayensis*, *D. dangila* (Engeszer et al., 2007)]. Fish were reared under standard conditions to maintain *D. rerio* (~28 °C; 14 L:10D) with larvae fed initially marine rotifers, derived from high-density cultures and enriched with Rotimac and Algamac (Reed Mariculture), with older larvae and adults subsequently fed live brine shrimp and a blend of flake foods enriched with dried spirulina. Stocks of mutant or transgenic *D. albolineatus* were: *scarb1*<sup>vp38ac1</sup>, *scarb1*<sup>vp38ac2</sup>, *cyp2ae2*<sup>vp39ac1</sup>, *bdh1*<sup>vp40ac1</sup>, *bdh1*<sup>vp40ac2</sup>, *csf1ra*<sup>vp4ac1</sup>, *Tg(aox5:nucEosFP)*<sup>vp43aTg</sup>.

CRISPR/Cas9 mutagenesis *bdh1a*<sup>vp40ac1</sup> and *cyp2ae2*<sup>vp39ac1</sup> were generated by injecting one-cell stage embryos with 200 pg sgRNAs and 500 pg Cas9 protein (PNA Bio) using standard procedures (Shah et al., 2015). *bco1*<sup>vp41ac1</sup>, *bco1*<sup>vp41ac2</sup>, *scarb1*<sup>vp38ac1</sup> and *scarb1*<sup>vp38ac2</sup> mutagenesis as well as *scarb1* targeted clonal labeling were conducted by injecting one-cell stage embryos with approximately 1 nanoliter of 5 μM gRNA:Cas9 RNP complex (IDT). These AltR CRISPR/Cas9 reagents allowed for highly efficient mutagenesis (Hoshijima et al., 2019) even in F0 fish, enabling clonal analyses of rare wild-type cells. For production of mutant lines, individual fish were sorted for anal fin phenotypes at juvenile stages and alleles recovered by intercrossing and outcrossing.

Transgenesis *aox5:nucEosFP* and *mitfa:nucEosFP* plasmids were made by assembling 8 kb *aox5* and 5 kb *mitfa* promoters (Budi et al., 2011; McMenamin et al., 2014) with nuclear-localizing photoconvertible fluorophore EosFP using the tol2 Gateway Kit (Kwan et al., 2007) and were injected at the one-cell stage with tol2 mRNA at 25 pg per embryo (Suster et al., 2009) or 6 pg per embryo for clonal analyses.

## Imaging and image processing

Whole fish were euthanized then embedded in 1 % low-melt agarose, and captured on a Nikon D-810 digital single lens reflex camera with MicroNikkor 105 mm macro lens. Anal fin details were imaged using a Zeiss Axio Observer inverted microscope or Zeiss AxioZoom stereomicroscope equipped with Zeiss Axiocam cameras.

Carotenoid autofluorescence was imaged using a Zeiss LSM880 inverted laser confocal microscope in Airyscan SR mode. Laser intensity for red (excitation wavelength 561 nm) and green (excitation wavelength 488 nm) channels were set to be identical. For comparison with brightfield illumination, anal fins were stabilized with a few drops of 1 % low-melt agarose then specimens transferred to a Zeiss AxioObserver inverted microscope with Axiocam camera. Cells along the mid line of 10th inter-fin ray were imaged. Background of bright-field images was corrected to white using software Fiji imageJ (Schindelin et al., 2012): Duplicate> Gaussian Blur = 50 > Image Calculator to subtract background> Invert. For larva to juvenile comparisons (Figure 1F), 10 cells in 3rd and 4th inter-fin ray in proximal and distal were imaged. For wild-type and mutant comparisons (Figure 7D), 20 cells in 10th inter-fin ray in proximal and distal were imaged. Other fluorescent images (e.g. photoconverted images, *aox5+* clonal labeling) were acquired using a Zeiss AxioObserver inverted microscope equipped with Yokogawa CSU-X1M5000 laser spinning disk and Hamatsu camera.

Images were captured either as single frames or as tiled sets of larger areas that were then stitched computationally using ZEN Blue software, the Autoblend feature of Adobe Photoshop, or manually in Adobe Photoshop. Color balance and display levels were adjusted manually for entire images as needed, with corresponding transformations applied across matched sets of images (e.g. across genotypes). In some instances, gradients of brightness across fields of view (e.g. proximal to distal) were adjusted by applying inverse density gradients in Adobe Photoshop.

## Fate mapping and lineage analysis

Photoconversion was performed on *Tg(aox5:nucEosFP)* or plasmid-injected F0 *mitfa:nucEosFP*, using a Zeiss LSM 800 scanning laser confocal with a 405 nm laser and ZEN blue software. Fish were subsequently reared in tanks shaded from ambient light to prevent spontaneous photoconversion



(McMenamin et al., 2014; Gur et al., 2020). Brightfield images were taken before photoconversion and fish inspected to ensure that no photoconversion had occurred as a result. Subsequent imaging used fluorescence channels only, except for end-point imaging in fluorescence followed by brightfield. Although pigments autofluoresce in the same channels as nucEosFP, treatment with epinephrine allowed contracted pigment granules to be distinguished unambiguously from nuclei.

For amputation experiments, fins were transected through the middle of the erythrofore-containing region, and imaged subsequently in brightfield (Figure 5A) following treatment with epinephrine. Alternatively, *Tg(aox5:nucEosFP)* adult males were exposed under an external Zeiss HXP 120 V compact light source for 15 min until all nucEosFP+ cells in fins had been converted (Figure 5C). Fish were anesthetized and anal fins amputated through erythrofore regions, then reared in a shaded tank as above. Unconverted controls reared in the same tank did not show any converted nucEosFP signal when examined concurrently at subsequent time points. Sham control (photoconverted without amputation) of regeneration experiment in Figure 5C. Converted nucEosFP signal remained very strong after 41 days. Images were taken 1 day after amputation and at the end point of the experiment. For excisions of middle fin regions (Figure 5—figure supplement 2), internal fin ray and inter-fin ray regions were removed and xanthophores close to the wound photoconverted.

### Reverse transcription polymerase chain reaction (RT-PCR) analysis

Adult male anal fins were dissected and dissociated enzymatically with Liberase (Sigma-Aldrich cat. 5401119001, 0.25 mg/mL in dPBS) at 25 °C for 15 min followed by gently pipetting for 5 min. Cell suspensions were then filtered through a 70 m Nylon cell strainer to obtain a single-cell suspension. Individual cells were then picked manually under Zeiss Axio Observer inverted microscope. Cells were identified by their morphology: red erythrofores, yellow xanthophores, black melanophores and transparent small skin cells. Total RNAs were isolated by RNeasy Protect Mini Kit (Qiagen) and cDNAs synthesized with oligo-dT priming using SuperScript III Cells Direct cDNA Synthesis System (Thermo). Primers pairs were designed to span exon-intron junctions or long introns for assessing genomic contamination, targeting (Supplementary file 1—Table 5). Amplifications were performed using Taq polymerase with 35 cycles of 95 °C for 30 s, 56 °C for 30 s, 72 °C for 15 s.

### Pteridine autofluorescence

To assess pteridine content, amputated fins were imaged after exposure to dilute ammonia (pH 10.0), which liberates pteridines from protein carriers resulting in autofluorescence under DAPI illumination.

### RNA-Seq

Adult male *Danio albolineatus* were euthanized, anal fins were dissected and tissue collected from proximal erythrofore or distal xanthophore regions in PBS. RNA was extracted using TRIzol and Direct-zol RNA MiniPrep Kit. mRNA was enriched using NEBNext Poly(A) mRNA Magnetic Isolation Module and sequencing libraries were constructed using NEBNext Ultra RNA Library Prep Kit for Illumina and sequenced on an Illumina Nextseq-500. Reads were aligned to *Danio rerio* reference genome GRCz11 using Kallisto (Bray et al., 2016) and analyzed using DESeq2 (Love et al., 2014). RNA-seq data are available through GEO (accession ID GSE174713).

### Carotenoid analyses

Proximal (erythrofore containing) and distal (xanthophore containing) portions of the anal fin were dissected from nine individuals of each genotype and like samples were combined in pools of three for pigment extraction. The pooled fin tissue was homogenized with zirconia beads in 1.2 ml of 0.9 % sodium chloride and protein content was quantified a bicinchoninic acid (BCA) assay (23250, Thermo). Carotenoids were extracted from the homogenates by combining 1 ml methanol, 2 ml distilled water, and 2 ml of hexane:tert-methyl butyl ether (1:1 vol:vol), collecting and drying the resulting solvent fraction under nitrogen. Each sample was then split and saponified with 0.02 M NaOH or 0.2 M NaOH in methanol at room temperature to maximize the recovery of ketocarotenoids or other xanthophylls, respectively (Toomey and McGraw, 2007). The saponified extracts were then injected into an Agilent 1,100 series HPLC fitted with a YMC carotenoid 5.0 µm column (4.6 mm × 250 mm, YMC). Carotenoids were separated with a gradient mobile phase of acetonitrile:methanol:dichloromethane (44:44:12) (vol:vol:vol) through 11 minutes, a ramp up to solvent ratios of 35:35:30 for 11–21 min and isocratic

conditions through 35 minutes. The column was maintained at 30 °C with a mobile phase flow rate of 1.2 ml min<sup>-1</sup> throughout. The samples were monitored with a photodiode array detector at 400, 445, and 480 nm, and carotenoids were identified and quantified by comparison to authentic standards (a gift of DSM Nutritional Products, Heerlen, The Netherlands).

## Statistical analyses

Analyses of quantitative data were performed in JMP Pro 16 (SAS Institute, Cary NC). Numerical data presented in figures are provided in **Supplementary file 1**.

## Acknowledgements

Supported by NIH R35 GM122471 to DMP and startup funds from the University of Tulsa to MBT. Thanks to Jin Liu and Samantha Sturiale for assistance with screening, stock propagation and imaging, Lauren Saunders and Andy Aman for assistance with RNA-Seq, and Amber Schwindling for fish husbandry.

---

## Additional information

### Funding

Funder	Grant reference number	Author
National Institute of General Medical Sciences	R35 GM122471	David M Parichy
University of Tulsa	start-up funds	Matthew B Toomey

The funders had no role in study design, data collection and interpretation, or the decision to submit the work for publication.

### Author contributions

Delai Huang, Conceptualization, Formal analysis, Investigation, Methodology, Supervision, Validation, Visualization, Writing - original draft, Writing – review and editing; Victor M Lewis, Matthew B Toomey, Investigation, Writing – review and editing; Tarah N Foster, Investigation; Joseph C Corbo, Supervision, Writing – review and editing; David M Parichy, Conceptualization, Data curation, Formal analysis, Funding acquisition, Investigation, Methodology, Project administration, Supervision, Validation, Visualization, Writing - original draft, Writing – review and editing

### Author ORCIDs

Matthew B Toomey  <http://orcid.org/0000-0001-9184-197X>  
Joseph C Corbo  <http://orcid.org/0000-0002-9323-7140>  
David M Parichy  <http://orcid.org/0000-0003-2771-6095>

### Ethics

This study was performed in strict accordance with the recommendations in the Guide for the Care and Use of Laboratory Animals of the National Institutes of Health. All of the animals were handled according to approved institutional Animal Care and Use Committee (ACUC) protocol (#4170) of the University of Virginia. Euthanasia was accomplished by overdose of MS222 followed by physical maceration.

### Decision letter and Author response

Decision letter <https://doi.org/10.7554/70253.sa1>

Author response <https://doi.org/10.7554/70253.sa2>

---

## Additional files

### Supplementary files

- Supplementary file 1. Tables of RNA-Seq analyses, reagents, and HPLC retention times.

- Transparent reporting form

### Data availability

Numerical data presented in figure panels are provided in Supplementary File 1. RNA-Seq data has been deposited in GEO and is publicly available, accession #GSE174713.

The following dataset was generated:

Author(s)	Year	Dataset title	Dataset URL	Database and Identifier
Huang D	2021	Development and genetics of red coloration in the zebrafish relative <i>Danio albolineatus</i>	<a href="http://www.ncbi.nlm.nih.gov/geo/query/acc.cgi?acc=GSE174713">http://www.ncbi.nlm.nih.gov/geo/query/acc.cgi?acc=GSE174713</a>	NCBI Gene Expression Omnibus, GSE174713

## References

- Ansai S**, Mochida K, Fujimoto S, Mokodongan DF, Sumarto BKA, Masengi KWA, Hadiaty RK, Nagano AJ, Toyoda A, Naruse K, Yamahira K, Kitano J. 2021. Genome editing reveals fitness effects of a gene for sexual dichromatism in Sulawesian fishes. *Nature Communications* **12**: 1350. DOI: <https://doi.org/10.1038/s41467-021-21697-0>, PMID: 33649298
- Asada M**. 1978. Presence of melanosome-like granules in dermal erythrophores of the tropical teleost (*Badis badis*). *Experientia* **34**: 511–512. DOI: <https://doi.org/10.1007/bf01935961>
- Bagnara JT**, Matsumoto J. 2006. Chapter 2. Comparative anatomy and physiology of pigment cells in nonmammalian tissues. Nordland JJ, Boissy RE, Hearing VJ, King RA, Oetting WS, Ortonne JP (Eds). *The Pigmentary System: Physiology and Pathophysiology*. New York, New York: Oxford University Press. p. 1–23. DOI: <https://doi.org/10.1002/9780470987100.ch2>
- Ballowitz E**. 1913. Über Schwarz-rote und Sternförmig Farbzellenkombinationen in der Haut von Gobiiden. Ein weiterer Beitrag zur Kenntnis der chromatophoren und Chromatophoren-vereinigungen knochenfischen. *Zeitschrift Für Wissenschaftliche Zoologie* **106**: 527–593.
- Bray NL**, Pimentel H, Melsted P, Pachter L. 2016. Near-optimal probabilistic RNA-seq quantification. *Nature Biotechnology* **34**: 525–527. DOI: <https://doi.org/10.1038/nbt.3519>, PMID: 27043002
- Brodie ED**, Brodie ED. 1980. Differential avoidance of mimetic salamanders by free-ranging birds. *Science* **208**: 181–182. DOI: <https://doi.org/10.1126/science.208.4440.181>, PMID: 17745538
- Budi EH**, Patterson LB, Parichy DM. 2011. Post-embryonic nerve-associated precursors to adult pigment cells: Genetic requirements and dynamics of morphogenesis and differentiation. *PLOS Genetics* **7**: e1002044. DOI: <https://doi.org/10.1371/journal.pgen.1002044>, PMID: 21625562
- Caro T**, Mallarino R. 2020. Coloration in mammals. *Trends in Ecology & Evolution* **35**: 357–366. DOI: <https://doi.org/10.1016/j.tree.2019.12.008>, PMID: 31980234
- Cruz-Miralles Á**, Avilés JM, Chastel O, Expósito-Granados M, Parejo D. 2020. Phaeomelanin matters: Redness associates with inter-individual differences in behaviour and feather corticosterone in male scops owls (*Otus scops*). *PLOS ONE* **15**: e0241380. DOI: <https://doi.org/10.1371/journal.pone.0241380>, PMID: 33175892
- Dijkstra PD**, Hemelrijk C, Seehausen O, Groothuis TGG. 2008. Color polymorphism and intrasexual competition in assemblages of cichlid fish. *Behavioral Ecology* **20**: 138–144. DOI: <https://doi.org/10.1093/beheco/arn125>
- Djurđević I**, Kreft ME, Sušnik Bajec S. 2015. Comparison of pigment cell ultrastructure and organisation in the dermis of marble trout and brown trout, and first description of erythrophore ultrastructure in salmonids. *Journal of Anatomy* **227**: 583–595. DOI: <https://doi.org/10.1111/joa.12373>, PMID: 26467239
- Dooley CM**, Mongera A, Walderich B, Nüsslein-Volhard C. 2013. On the embryonic origin of adult melanophores: The role of *erbb* and *kit* signalling in establishing melanophore stem cells in zebrafish. *Development* **140**: 1003–1013. DOI: <https://doi.org/10.1242/dev.087007>, PMID: 23364329
- Endler JA**. 1980. Natural-selection on color patterns in *poecilia reticulata*. *Evolution; International Journal of Organic Evolution* **34**: 76–91. DOI: <https://doi.org/10.1111/j.1558-5646.1980.tb04790.x>, PMID: 28563214
- Engeszer RE**, Patterson LB, Rao AA, Parichy DM. 2007. Zebrafish in the wild: A review of natural history and new notes from the field. *Zebrafish* **4**: 21–40. DOI: <https://doi.org/10.1089/zeb.2006.9997>, PMID: 18041940
- Evans MR**, Norris K. 1996. The importance of carotenoids in signaling during aggressive interactions between male firemouth cichlids (*Cichlasoma meeki*). *Behavioral Ecology* **7**: 1–6. DOI: <https://doi.org/10.1093/beheco/7.1.1>
- Fang F**, Kottelat M. 2000. *Danio roseus*, a new species from the Mekong basin in northeastern Thailand and northwestern Laos (Teleostei: Cyprinidae). *Ichthyol Explor Freshwaters* **11**: 149–154.
- Ghyselinck NB**, Duester G. 2019. Retinoic acid signaling pathways. *Development* **146**: dev.167502. DOI: <https://doi.org/10.1242/dev.167502>, PMID: 31273085
- Goda M**, Fujii R. 1995. Blue chromatophores in two species of callionymid fish. *Zoological Science* **12**: 811–813. DOI: <https://doi.org/10.2108/Zsj.12.811>
- Goda M**, Ohata M, Ikoma H, Fujiyoshi Y, Sugimoto M, Fujii R. 2011. Integumental reddish-violet coloration owing to novel dichromatic chromatophores in the teleost fish, pseudochromis diadema. *Pigment Cell & Melanoma Research* **24**: 614–7.

- Goda M**, Fujiyoshi Y, Sugimoto M, Fujii R. 2013. Novel dichromatic chromatophores in the integument of the Mandarin fish *Synchiropus splendidus*. *The Biological Bulletin* **224**: 14–17. DOI: <https://doi.org/10.1086/BBLv224n1p14>
- Godin JGJ**, McDonough HE. 2003. Predator preference for brightly colored males in the Guppy: A viability cost for a sexually selected trait. *Behavioral Ecology* **14**: 194–200. DOI: <https://doi.org/10.1093/beheco/14.2.194>
- Goodrich HB**, Hill GA, Arrick MS. 1941. The chemical identification of gene-controlled pigments in *Platyopceilus* and xiphophorus and comparisons with other tropical fish. *Genetics* **26**: 573–586 PMID: 17247023.,
- Goodrich HB**, Greene JM. 1959. An experimental analysis of the development of a color pattern in the fish brachydanio *Albolineatus blyth*. *The Journal of Experimental Zoology* **141**: 15–45. DOI: <https://doi.org/10.1002/jez.1401410103>, PMID: 13851086
- Granneman JG**, Kimler VA, Zhang H, Ye X, Luo X, Postlethwait JH, Thummel R. 2017. Lipid droplet biology and evolution illuminated by the characterization of a novel perilipin in teleost fish. *eLife* **6**: e21771. DOI: <https://doi.org/10.7554/eLife.21771>, PMID: 28244868
- Green D**, Marks AR, Fleischer S, McIntyre JO. 1996. Wild type and mutant human heart (r)-3-hydroxybutyrate dehydrogenase expressed in insect cells. *Biochemistry* **35**: 8158–8165. DOI: <https://doi.org/10.1021/bi952807n>, PMID: 8679568
- Grether GF**. 2000. Carotenoid limitation and mate preference evolution: a test of the indicator hypothesis in guppies (*Poecilia reticulata*). *Evolution; International Journal of Organic Evolution* **54**: 1712–1724. DOI: <https://doi.org/10.1111/j.0014-3820.2000.tb00715.x>, PMID: 11108598
- Grether GF**, Hudon J, Endler JA. 2001. Carotenoid scarcity, synthetic pteridine pigments and the evolution of sexual coloration in guppies (*Poecilia reticulata*). *Proceedings. Biological Sciences* **268**: 1245–1253. DOI: <https://doi.org/10.1098/rspb.2001.1624>, PMID: 11410150
- Gur D**, Bain EJ, Johnson KR, Aman AJ, Pasoili HA, Flynn JD, Allen MC, Deheyn DD, Lee JC, Lippincott-Schwartz J, Parichy DM. 2020. In situ differentiation of iridophore crystalloids underlies zebrafish stripe patterning. *Nature Communications* **11**: 6391. DOI: <https://doi.org/10.1038/s41467-020-20088-1>, PMID: 33319779
- Harrison EH**, Kopec RE. 2020. Enzymology of vertebrate carotenoid oxygenases. *Biochim Biophys Acta Mol Cell Biol Lipids* **1865**: 158653. DOI: <https://doi.org/10.1016/j.bbalip.2020.158653>
- Hill GE**. 1991. Plumage coloration is a sexually selected indicator of male quality. *Nature* **350**: 337–339. DOI: <https://doi.org/10.1038/350337a0>
- Hirata M**, Nakamura K, Kanemaru T, Shibata Y, Kondo S. 2003. Pigment cell organization in the hypodermis of zebrafish. *Developmental Dynamics* **227**: 497–503. DOI: <https://doi.org/10.1002/dvdy.10334>, PMID: 12889058
- Hoshijima K**, Jurynek MJ, Klatt Shaw D, Jacobi AM, Behlke MA, Grunwald DJ. 2019. Highly Efficient CRISPR-Cas9-Based Methods for Generating Deletion Mutations and F0 Embryos that Lack Gene Function in Zebrafish. *Developmental Cell* **51**: e4. DOI: <https://doi.org/10.1016/j.devcel.2019.10.004>
- Houde AE**. 1997. *Sex, Color, and Mate Choice in Guppies*. Princeton, NJ: Princeton University Press.
- Hubbard JK**, Uy JAC, Hauber ME, Hoekstra HE, Safran RJ. 2010. Vertebrate pigmentation: From underlying genes to adaptive function. *Trends in Genetics* **26**: 231–239. DOI: <https://doi.org/10.1016/j.tig.2010.02.002>, PMID: 20381892
- Ichikawa Y**, Ohtani H, Miura I. 1998. The erythrophore in the larval and adult dorsal skin of the brown frog, *Rana ornativentris*: Its differentiation, migration, and pigmentary organelle formation. *Pigment Cell Research* **11**: 345–354. DOI: <https://doi.org/10.1111/j.1600-0749.1998.tb00493.x>, PMID: 9870546
- Ide H**, Hama T. 1976. Transformation of amphibian iridophores into melanophores in clonal culture. *Developmental Biology* **53**: 297–302. DOI: [https://doi.org/10.1016/0012-1606\(76\)90232-3](https://doi.org/10.1016/0012-1606(76)90232-3), PMID: 1086809
- Johnson S**, Candolin U. 2017. Predation cost of a sexual signal in the threespine stickleback. *Behavioral Ecology* **28**: 1160–1165. DOI: <https://doi.org/10.1093/beheco/axx080>
- Kelsh RN**, Harris ML, Colanesi S, Erickson CA. 2009. stripes and belly-spots -- a review of pigment cell morphogenesis in vertebrates. *Seminars in Cell & Developmental Biology* **20**: 90–104. DOI: <https://doi.org/10.1016/j.semcdb.2008.10.001>, PMID: 18977309
- Khalil S**, Welklin JF, McGraw KJ, Boersma J, Schwabl H, Webster MS, Karubian J. 2020. Testosterone regulates CYP2J19-linked carotenoid signal expression in male red-backed fairywrens (*Malurus melanocephalus*). *Proceedings. Biological Sciences* **287**: 20201687. DOI: <https://doi.org/10.1098/rspb.2020.1687>, PMID: 32933448
- Khoo G**, Lim TM, Phang VPE. 2012. Ultrastructure of erythrophores and xanthophores of the Siamese fighting fish, *Betta splendens*. *Isr J Aquacult-Bamid* **64**: 775. DOI: <https://doi.org/10.46989/001c.20620>
- Kirschian N**, McArthur AG, Jesuthasan C, Krattenmacher B, Wilson JY. 2011. Phylogenetic and functional analysis of the vertebrate Cytochrome p450 2 family. *Journal of Molecular Evolution* **72**: 56–71. DOI: <https://doi.org/10.1007/s00239-010-9402-7>, PMID: 21116621
- Kullander SO**, Fang F. 2009. *Danio tinwini*, a new species of spotted danio from northern Myanmar (Teleostei: Cyprinidae). *Ichthyol Explor Freshw* **20**: 223–228.
- Kullander SO**. 2012. Description of *Danio flagrans*, and redescription of *D. choprae*, two closely related species from the Ayeyarwaddy River drainage in northern Myanmar (Teleostei: Cyprinidae). *Ichthyol Explor Freshw* **23**: 245–262.
- Kullander SO**, Rahman MM, Norén M, Mollah AR. 2015. *Danio annulosus*, a new species of chain Danio from the Shuvolong Falls in Bangladesh (Teleostei: Cyprinidae: Danioninae). *Zootaxa* **3994**: 53–68. DOI: <https://doi.org/10.11646/zootaxa.3994.1.2>, PMID: 26250259

- Kullander SO**, Norén M. 2016. Danio htamanthinus (Teleostei: Cyprinidae), a new species of miniature cyprinid fish from the Chindwin River in Myanmar. *Zootaxa* **4178**: 535–546. DOI: <https://doi.org/10.11646/zootaxa.4178.4.5>, PMID: 27811706
- Kwan KM**, Fujimoto E, Grabher C, Mangum BD, Hardy ME, Campbell DS, Parant JM, Yost HJ, Kanki JP, Chien CB. 2007. The TOL2KIT: A multisite gateway-based construction kit for Tol2 transposon transgenesis constructs. *Developmental Dynamics* **236**: 3088–3099. DOI: <https://doi.org/10.1002/dvdy.21343>, PMID: 17937395
- Langston HP**, Jones L, Churchill S, Churchill PF. 1996. Purification and characterization of a (r)-3-hydroxybutyrate dehydrogenase deletion mutant. Evidence for c-terminal involvement in enzyme activation by lecithin. *Archives of Biochemistry and Biophysics* **327**: 45–52. DOI: <https://doi.org/10.1006/abbi.1996.0091>, PMID: 8615695
- Lewis VM**, Saunders LM, Larson TA, Bain EJ, Sturiale SL, Gur D, Chowdhury S, Flynn JD, Allen MC, Deheyn DD, Lee JC, Simon JA, Lippincott-Schwartz J, Raible DW, Parichy DM. 2019. Fate plasticity and reprogramming in genetically distinct populations of Danio leucophores. *PNAS* **116**: 11806–11811. DOI: <https://doi.org/10.1073/pnas.1901021116>, PMID: 31138706
- Li B**, Vachali PP, Shen Z, Gorusupudi A, Nelson K, Besch BM, Bartschi A, Longo S, Mattinson T, Shihab S, Polyakov NE, Suntsova LP, Dushkin AV, Bernstein PS. 2017. Retinal accumulation of zeaxanthin, lutein, and  $\beta$ -carotene in mice deficient in carotenoid cleavage enzymes. *Experimental Eye Research* **159**: 123–131. DOI: <https://doi.org/10.1016/j.exer.2017.02.016>, PMID: 28286282
- Lister JA**, Robertson CP, Lepage T, Johnson SL, Raible DW. 1999. Nacre encodes a zebrafish microphthalmia-related protein that regulates neural-crest-derived pigment cell fate. *Development* **126**: 3757–3767 PMID: 10433906.
- Lister JA**. 2019. Larval but not adult xanthophore pigmentation in zebrafish requires GTP cyclohydrolase 2 (gch2) function. *Pigment Cell & Melanoma Research* **32**: 724–727. DOI: <https://doi.org/10.1111/pcmr.12783>
- Lopes RJ**, Johnson JD, Toomey MB, Ferreira MS, Araujo PM, Melo-Ferreira J, Andersson L, Hill GE, Corbo JC, Carneiro M. 2016. Genetic basis for red coloration in birds. *Current Biology* **26**: 1427–1434. DOI: <https://doi.org/10.1016/j.cub.2016.03.076>, PMID: 27212400
- Love MI**, Huber W, Anders S. 2014. Moderated estimation of fold change and dispersion for RNA-seq data with DESeq2. *Genome Biology* **15**: 550. DOI: <https://doi.org/10.1186/s13059-014-0550-8>, PMID: 25516281
- Matsumoto J**. 1965. Studies on fine structure and cytochemical properties of erythrocytes in swordtail, *Xiphophorus helleri*, with special reference to their pigment granules (Pterinosomes). *The Journal of Cell Biology* **27**: 493–504. DOI: <https://doi.org/10.1083/jcb.27.3.493>, PMID: 5885426
- Matsumoto J**, Obika M. 1968. Morphological and biochemical characterization of goldfish erythrocytes and their pterinosomes. *The Journal of Cell Biology* **39**: 233–250. DOI: <https://doi.org/10.1083/jcb.39.2.233>, PMID: 5692582
- McClure MM**, McIntyre PB, McCune AR. 2006. Notes on the natural diet and habitat of eight danionin fishes, including the zebrafish *Danio rerio*. *Journal of Fish Biology* **69**: 553–570. DOI: <https://doi.org/10.1111/j.1095-8649.2006.01125.x>
- McCluskey BM**, Postlethwait JH. 2015. Phylogeny of zebrafish, a “model species,” within Danio, a “model genus”. *Molecular Biology and Evolution* **32**: 635–652. DOI: <https://doi.org/10.1093/molbev/msu325>, PMID: 25415969
- McCluskey BM**, Uji S, Mancusi JL, Postlethwait JH, Parichy DM. 2021. A complex genetic architecture in zebrafish relatives *Danio Quagga* and *D. KYATHIT* underlies development of stripes and spots. *PLOS Genetics* **17**: e1009364. DOI: <https://doi.org/10.1371/journal.pgen.1009364>, PMID: 33901178
- McGraw KJ**, Safran RJ, Wakamatsu K. 2005. How feather colour reflects its melanin content. *Functional Ecology* **19**: 816–821. DOI: <https://doi.org/10.1111/j.1365-2435.2005.01032.x>
- McGraw KJ**. 2006. Mechanics of Carotenoid-Based Coloration. Bird Coloration Volume I Mechanisms and Measurements. Cambridge MA: Harvard University Press.
- McMenamin SK**, Bain EJ, McCann AE, Patterson LB, Eom DS, Waller ZP, Hamill JC, Kuhlman JA, Eisen JS, Parichy DM. 2014. Thyroid hormone-dependent adult pigment cell lineage and pattern in zebrafish. *Science* **345**: 1358–1361. DOI: <https://doi.org/10.1126/science.1256251>, PMID: 25170046
- Milinski M**, Bakker TCM. 1990. Female sticklebacks use male coloration in mate choice and hence avoid parasitized males. *Nature* **344**: 330–333. DOI: <https://doi.org/10.1038/344330a0>
- Mundy NI**, Stapley J, Bennison C, Tucker R, Twyman H, Kim KW, Burke T, Birkhead TR, Andersson S, Slate J. 2016. Red Carotenoid Coloration in the Zebra Finch Is Controlled by a Cytochrome P450 Gene Cluster. *Current Biology* **26**: 1435–1440. DOI: <https://doi.org/10.1016/j.cub.2016.04.047>
- Niu MC**. 1954. Further studies on the origin of amphibian pigment cells. *Journal of Experimental Zoology* **125**: 199–220. DOI: <https://doi.org/10.1002/jez.1401250203>
- Odenthal J**, Rossnagel K, Haffter P, Kelsh RN, Vogelsang E, Brand M, van Eeden FJM, Furutani-Seiki M, Granato M, Hammerschmidt CP, Jiang YJ, Kane DA, Kelsh RN, Mullins MC, Nusslein-Volhard C. 1996. Mutations affecting xanthophore pigmentation in the zebrafish, *Danio rerio*. *Development* **123**: 391–398 PMID: 9007257.
- Olsson M**, Stuart-Fox D, Ballen C. 2013. Genetics and evolution of colour patterns in reptiles. *Seminars in Cell & Developmental Biology* **24**: 529–541. DOI: <https://doi.org/10.1016/j.semcdb.2013.04.001>, PMID: 23578866
- Oshima N**, Kasai A. 2002. Iridophores involved in generation of skin color in the zebrafish, *Brachy Danio rerio*. *Forma* **17**: 91–101.
- Otsuka H**, Kimura T, Ago Y, Nakama M, Aoyama Y, Abdelkreem E, Matsumoto H, Ohnishi H, Sasai H, Osawa M, Yamaguchi S, Mitchell GA, Fukao T. 2020. Deficiency of 3-hydroxybutyrate dehydrogenase (bdh1) in mice

- causes low ketone body levels and fatty liver during fasting. *Journal of Inherited Metabolic Disease* **43**: 960–968. DOI: <https://doi.org/10.1002/jimd.12243>, PMID: 32279332
- Parichy DM**, Ransom DG, Paw B, Zon LI, Johnson SL. 2000. An orthologue of the kit-related gene *fms* is required for development of neural crest-derived xanthophores and a subpopulation of adult melanocytes in the zebrafish, *Danio rerio*. *Development* **127**: 3031–3044. PMID: 10862741.
- Parichy DM**, Turner JM. 2003. Temporal and cellular requirements for FMS signaling during zebrafish adult pigment pattern development. *Development* **130**: 817–833. DOI: <https://doi.org/10.1242/dev.00307>, PMID: 12538511
- Parichy DM**. 2021. Evolution of pigment cells and patterns: Recent insights from teleost fishes. *Current Opinion in Genetics & Development* **69**: 88–96. DOI: <https://doi.org/10.1016/j.gde.2021.02.006>, PMID: 33743392
- Patterson LB**, Parichy DM. 2019. Zebrafish pigment pattern formation: Insights into the development and evolution of adult form. *Annual Review of Genetics* **53**: 505–530. DOI: <https://doi.org/10.1146/annurev-genet-112618-043741>, PMID: 31509458
- Persson B**, Kallberg Y, Bray JE, Bruford E, Dellaporta SL, Favia AD, Duarte RG, Jörnvall H, Kavanagh KL, Kedishvili N, Kisiela M, Maser E, Mindnich R, Orchard S, Penning TM, Thornton JM, Adamski J, Oppermann U. 2009. The SDR (short-chain dehydrogenase/reductase and related enzymes) nomenclature initiative. *Chemico-Biological Interactions* **178**: 94–98. DOI: <https://doi.org/10.1016/j.cbi.2008.10.040>, PMID: 19027726
- Poliakov E**, Uppal S, Rogozin IB, Gentleman S, Redmond TM. 2020. Evolutionary aspects and enzymology of metazoan carotenoid cleavage oxygenases. *Biochimica et Biophysica Acta. Molecular and Cell Biology of Lipids* **1865**: 158665. DOI: <https://doi.org/10.1016/j.bbalip.2020.158665>, PMID: 32061750
- Pryke SR**, Griffith SC. 2006. Red dominates black: Agonistic signalling among head morphs in the colour polymorphic gouldian finch. *Proceedings. Biological Sciences* **273**: 949–957. DOI: <https://doi.org/10.1098/rspb.2005.3362>, PMID: 16627280
- Quigley IK**, Manuel JL, Roberts RA, Nuckels RJ, Herrington ER, MacDonald EL, Parichy DM. 2005. Evolutionary diversification of pigment pattern in danio fishes: Differential FMS dependence and stripe loss in *D. albolineatus*. *Development* **132**: 89–104. DOI: <https://doi.org/10.1242/dev.01547>, PMID: 15563521
- Salis P**, Lorin T, Lewis V, Rey C, Marcionetti A, Escande M-L, Roux N, Besseau L, Salamin N, Sémon M, Parichy D, Volff J-N, Laudet V. 2019. Developmental and comparative transcriptomic identification of iridophore contribution to white barring in clownfish. *Pigment Cell & Melanoma Research* **32**: 391–402. DOI: <https://doi.org/10.1111/pcmr.12766>, PMID: 30633441
- Saunders LM**, Mishra AK, Aman AJ, Lewis VM, Toomey MB, Packer JS, Qiu X, McFaline-Figueroa JL, Corbo JC, Trapnell C, Parichy DM. 2019. Thyroid hormone regulates distinct paths to maturation in pigment cell lineages. *eLife* **8**: e45181. DOI: <https://doi.org/10.7554/eLife.45181>, PMID: 31140974
- Schartl M**, Larue L, Goda M, Bosenberg MW, Hashimoto H, Kelsh RN. 2016. What is a vertebrate pigment cell? *Pigment Cell & Melanoma Research* **29**: 8–14. DOI: <https://doi.org/10.1111/pcmr.12409>, PMID: 26247887
- Schindelin J**, Arganda-Carreras I, Frise E, Kaynig V, Longair M, Pietzsch T, Preibisch S, Rueden C, Saalfeld S, Schmid B, Tinevez JY, White DJ, Hartenstein V, Eliceiri K, Tomancak P, Cardona A. 2012. Fiji: An open-source platform for biological-image analysis. *Nature Methods* **9**: 676–682. DOI: <https://doi.org/10.1038/nmeth.2019>, PMID: 22743772
- Sefc KM**, Brown AC, Clotfelter ED. 2014. Carotenoid-based coloration in cichlid fishes. *Comparative Biochemistry and Physiology. Part A, Molecular & Integrative Physiology* **173C**: 42–51. DOI: <https://doi.org/10.1016/j.cbpa.2014.03.006>, PMID: 24667558
- Shah AN**, Davey CF, Whitebirch AC, Miller AC, Moens CB. 2015. Rapid reverse genetic screening using CRISPR in zebrafish. *Nature Methods* **12**: 535–540. DOI: <https://doi.org/10.1038/nmeth.3360>, PMID: 25867848
- Singh AP**, Schach U, Nüsslein-Volhard C. 2014. Proliferation, dispersal and patterned aggregation of iridophores in the skin prefigure striped colouration of zebrafish. *Nature Cell Biology* **16**: 607–614. DOI: <https://doi.org/10.1038/ncb2955>, PMID: 24776884
- Singh AP**, Dinwiddie A, Mahalwar P, Schach U, Linker C, Irion U, Nüsslein-Volhard C. 2016. Pigment cell progenitors in zebrafish remain multipotent through metamorphosis. *Developmental Cell* **38**: 316–330. DOI: <https://doi.org/10.1016/j.devcel.2016.06.020>, PMID: 27453500
- Slominski A**, Wortsman J, Plonka PM, Schallreuter KU, Paus R, Tobin DJ. 2005. Hair follicle pigmentation. *J Invest Dermatol* **124**: 13–21. DOI: <https://doi.org/10.1111/j.0022-202X.2004.23528.x>
- Spiewak JE**, Bain EJ, Liu J, Kou K, Sturiale SL, Patterson LB, Diba P, Eisen JS, Braasch I, Ganz J, Parichy DM. 2018. Evolution of endothelin signaling and diversification of adult pigment pattern in danio fishes. *PLoS Genetics* **14**: e1007538. DOI: <https://doi.org/10.1371/journal.pgen.1007538>, PMID: 30226839
- Stevens M**, Ruxton GD. 2012. Linking the evolution and form of warning coloration in nature. *Proceedings. Biological Sciences* **279**: 417–426. DOI: <https://doi.org/10.1098/rspb.2011.1932>, PMID: 22113031
- Strange C**. 2016. Carotenoids in Nature: Biosynthesis, Regulation and Function. Switzerland: Springer. DOI: <https://doi.org/10.1007/978-3-319-39126-7>
- Suster ML**, Kikuta H, Urasaki A, Asakawa K, Kawakami K. 2009. Transgenesis in zebrafish with the *tol2* transposon system. *Methods in Molecular Biology* **561**: 41–63. DOI: [https://doi.org/10.1007/978-1-60327-019-9\\_3](https://doi.org/10.1007/978-1-60327-019-9_3), PMID: 19504063
- Svensson PA**, Wong BBM. 2011. Carotenoid-based signals in behavioural ecology: A review. *Behaviour* **148**: 131–189. DOI: <https://doi.org/10.1163/000579510x548673>
- Tadokoro R**, Takahashi Y. 2017. Intercellular transfer of organelles during body pigmentation. *Current Opinion in Genetics & Development* **45**: 132–138. DOI: <https://doi.org/10.1016/j.gde.2017.05.001>, PMID: 28605672

- Takahashi D.** 2018. Female mate choice based on male nuptial coloration in pale chub, Zacco Platypus. *Zoological Science* **35**: 23–27. DOI: <https://doi.org/10.2108/zs170102>, PMID: 29417889
- Tang KL, Agnew MK, Hirt MV, Sado T, Schneider LM, Freyhof J, Sulaiman Z, Swartz E, Vidthayanon C, Miya M, Saitoh K, Simons AM, Wood RM, Mayden RL.** 2010. Systematics of the subfamily Danioninae (Teleostei: Cypriniformes: Cyprinidae). *Molecular Phylogenetics and Evolution* **57**: 189–214. DOI: <https://doi.org/10.1016/j.ympev.2010.05.021>
- Toews DPL, Hofmeister NR, Taylor SA.** 2017. The evolution and genetics of carotenoid processing in animals. *Trends in Genetics* **33**: 171–182. DOI: <https://doi.org/10.1016/j.tig.2017.01.002>, PMID: 28174022
- Toomey MB, McGraw KJ.** 2007. Modified saponification and HPLC methods for analyzing carotenoids from the retina of Quail: Implications for its use as a nonprimate model species. *Investigative Ophthalmology & Visual Science* **48**: 3976–3982. DOI: <https://doi.org/10.1167/iovs.07-0208>, PMID: 17724175
- Toomey MB, Lopes RJ, Araújo PM, Johnson JD, Gazda MA, Afonso S, Mota PG, Koch RE, Hill GE, Corbo JC, Carneiro M.** 2017. High-density lipoprotein receptor SCARB1 is required for carotenoid coloration in birds. *PNAS* **114**: 5219–5224. DOI: <https://doi.org/10.1073/pnas.1700751114>, PMID: 28465440
- Toomey MB, Marques CI, Andrade P, Araújo PM, Sabatino S, Gazda MA, Afonso S, Lopes RJ, Corbo JC, Carneiro M.** 2018. A non-coding region near follistatin controls head colour polymorphism in the Gouldian finch. *Proceedings. Biological Sciences* **285**: 1788. DOI: <https://doi.org/10.1098/rspb.2018.1788>, PMID: 30282656
- Tryon RC, Higdon CW, Johnson SL.** 2011. Lineage relationship of direct-developing melanocytes and melanocyte stem cells in the zebrafish. *PLOS ONE* **6**: e21010. DOI: <https://doi.org/10.1371/journal.pone.0021010>, PMID: 21698209
- Tu S, Johnson SL.** 2010. Clonal analyses reveal roles of organ founding stem cells, melanocyte stem cells and melanoblasts in establishment, growth and regeneration of the adult zebrafish fin. *Development* **137**: 3931–3939. DOI: <https://doi.org/10.1242/dev.057075>, PMID: 20980402
- Tu S, Johnson SL.** 2011. Fate restriction in the growing and regenerating zebrafish fin. *Developmental Cell* **20**: 725–732. DOI: <https://doi.org/10.1016/j.devcel.2011.04.013>, PMID: 21571228
- Twyman H, Valenzuela N, Literman R, Andersson S, Mundy NI.** 2016. Seeing red to being red: Conserved genetic mechanism for red cone oil droplets and co-option for red coloration in birds and turtles. *Proceedings. Biological Sciences* **283**: 1208. DOI: <https://doi.org/10.1098/rspb.2016.1208>, PMID: 27488652
- Twyman H, Andersson S, Mundy NI.** 2018. Evolution of CYP2J19, a gene involved in colour vision and red coloration in birds: Positive selection in the face of conservation and pleiotropy. *BMC Evolutionary Biology* **18**: 22. DOI: <https://doi.org/10.1186/s12862-018-1136-y>, PMID: 29439676
- von Lintig J, Hessel S, Isken A, Kiefer C, Lampert JM, Voolstra O, Vogt K.** 2005. Towards a better understanding of carotenoid metabolism in animals. *Biochimica et Biophysica Acta* **1740**: 122–131. DOI: <https://doi.org/10.1016/j.bbadis.2004.11.010>, PMID: 15949678
- Weaver RJ, Koch RE, Hill GE.** 2017. What maintains signal honesty in animal colour displays used in mate choice? *Philosophical Transactions of the Royal Society of London. Series B, Biological Sciences* **372**: 0343. DOI: <https://doi.org/10.1098/rstb.2016.0343>, PMID: 28533460
- Weaver RJ, Santos ESA, Tucker AM, Wilson AE, Hill GE.** 2018. Carotenoid metabolism strengthens the link between feather coloration and individual quality. *Nature Communications* **9**: 73. DOI: <https://doi.org/10.1038/s41467-017-02649-z>, PMID: 29311592
- Wedekind C, Meyer P, Frischknecht M, Niggli UA, Pfander H.** 1998. Different carotenoids and potential information content of red coloration of male three-spined stickleback. *Journal of Chemical Ecology* **24**: 787–801. DOI: <https://doi.org/10.1023/a:1022365315836>
- Weiss SL, Foerster K, Hudon J.** 2012. Pteridine, not carotenoid, pigments underlie the female-specific orange ornament of striped plateau lizards (*Sceloporus virgatus*). *Comparative Biochemistry and Physiology Part B* **161**: 117–123. DOI: <https://doi.org/10.1016/j.cbpb.2011.10.004>
- Widjaja-Adhi MAK, Lobo GP, Golczak M, Von Lintig J.** 2015. A genetic dissection of intestinal fat-soluble vitamin and carotenoid absorption. *Human Molecular Genetics* **24**: 3206–3219. DOI: <https://doi.org/10.1093/hmg/ddv072>, PMID: 25701869
- Yates AD, Achuthan P, Akanni W, Allen J, Allen J, Alvarez-Jarreta J, Amode MR, Armean IM, Azov AG, Bennett R, Bhai J, Billis K, Boddu S, Marugán JC, Cummins C, Davidson C, Dodiya K, Fatima R, Gall A, Giron CG, et al.** 2020. Ensembl 2020. *Nucleic Acids Research* **48**: D682–D688. DOI: <https://doi.org/10.1093/nar/gkz966>, PMID: 31691826
- Ziegler I.** 2003. The pteridine pathway in zebrafish: Regulation and specification during the determination of neural crest cell-fate. *Pigment Cell Research* **16**: 172–182. DOI: <https://doi.org/10.1034/j.1600-0749.2003.00044.x>, PMID: 12753383



---

## Figures and figure supplements

Development and genetics of red coloration in the zebrafish relative  
*Danio albolineatus*

**Delai Huang et al**



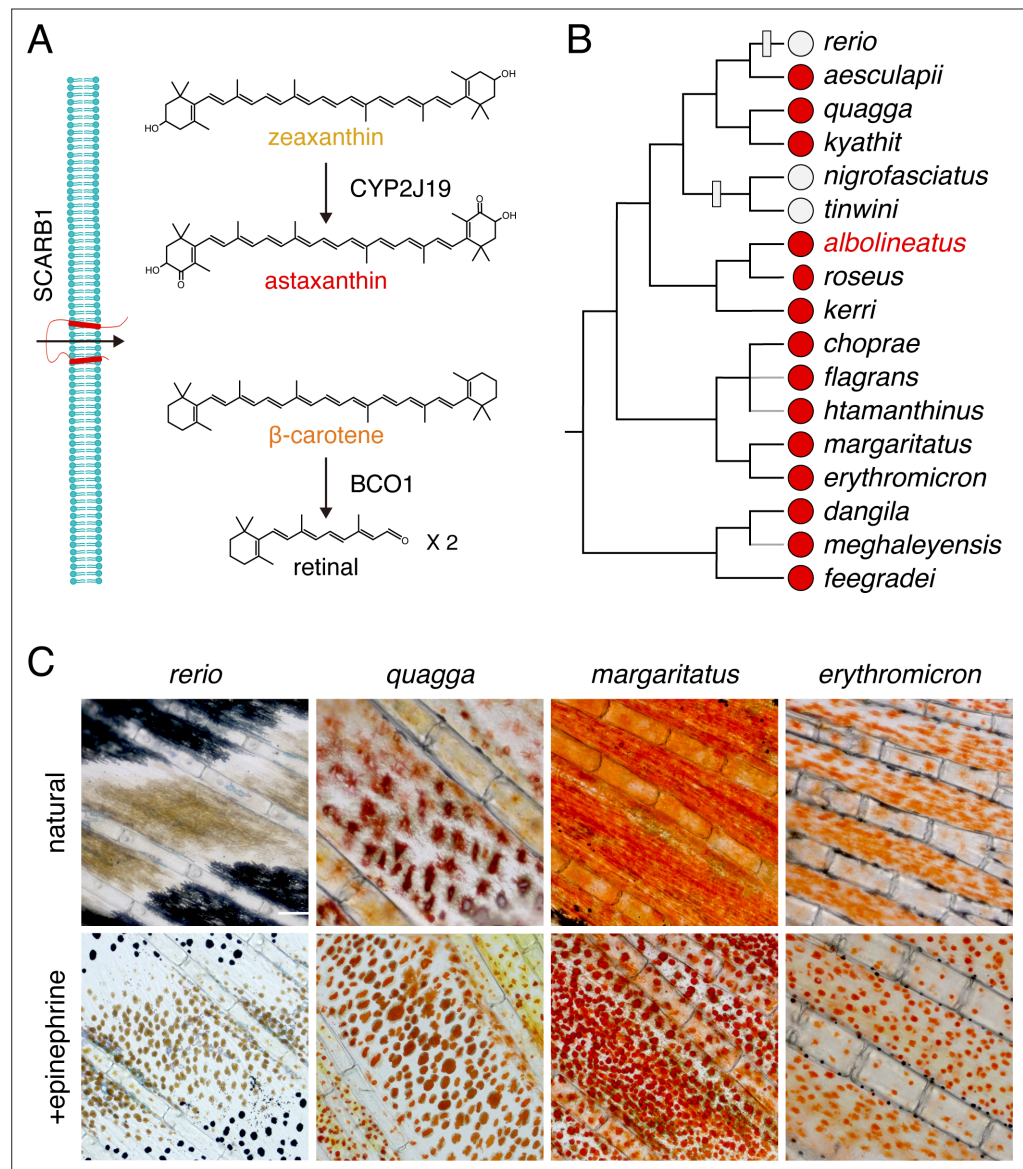


**Figure 1.** Carotenoid types and distribution of red erythrophores among *Danio* species. **(A)** Examples of major carotenoid types including yellow zeaxanthin, red astaxanthin, and orange  $\beta$ -carotene, with factors required for entry into cells and chemical modification (Main text). **(B)** Erythrophore presence (red circles) or absence (light gray circles) indicated by direct observation or prior species descriptions (Fang and Kottelat, 2000; Quigley et al., 2005; Engeszer et al., 2007; Kullander and Fang, 2009; Kullander, 2012; Kullander and Norén, 2016; Spiewak et al., 2018; McCluskey et al., 2021). A composite phylogeny based on several molecular evolutionary studies is shown; gray branches indicate lineage placements inferred by morphology alone (Tang et al., 2010; Kullander, 2012; Kullander et al., 2015; McCluskey and Postlethwait, 2015). Gray boxes across branches indicate lineages in which erythrophores are inferred most parsimoniously to have been lost. **(C)** Anal fin details of zebrafish (*rerio*) without erythrophores and other species with erythrophores. Cells are shown in their typical native states, with pigment dispersed, and following treatment with epinephrine, which causes pigment to be contracted toward cell centers. Scale bar: 100  $\mu$ m.

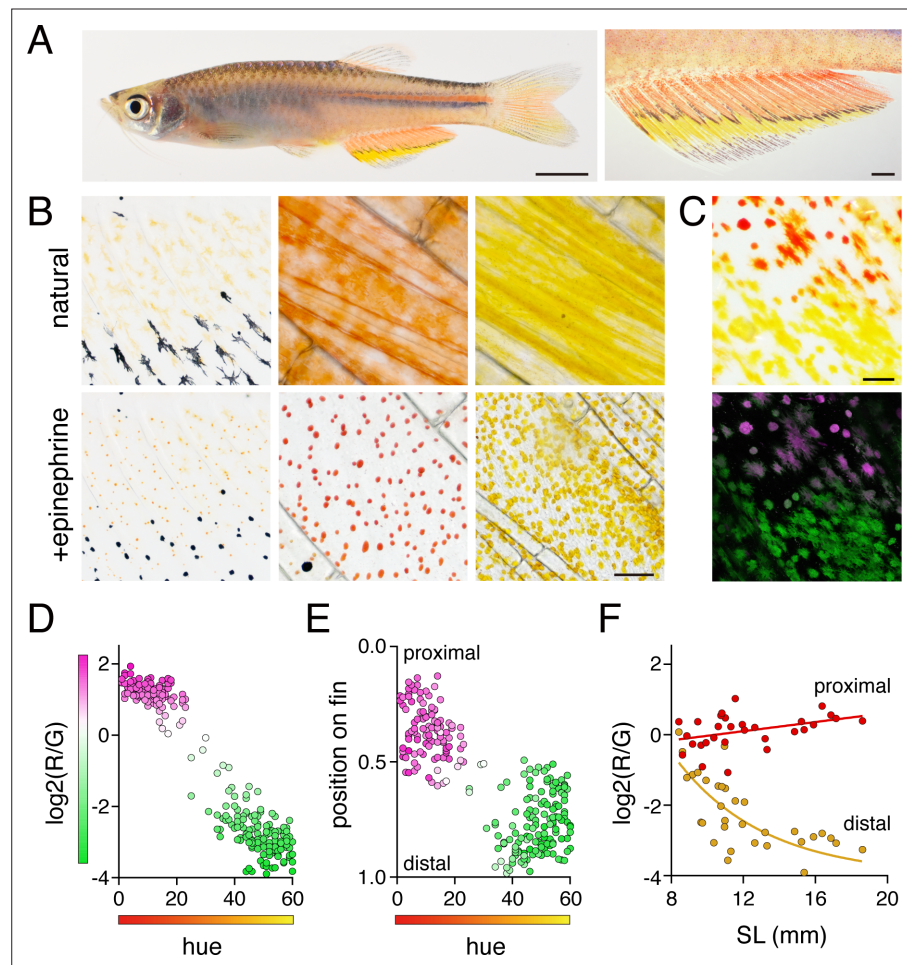


**Figure 2.** Anal fin pigment pattern of *D. albolineatus* and its ontogeny. (A) Erythrocytes were present on the body and were particularly evident on the anal fin (closeup at right), where these cells were found more proximally than yellow xanthophores. (B) At larval stages xanthophore-like cells with a uniform orange coloration occurred across the entire fin (left panels). Later in the adult, proximal red erythrocytes and distal yellow xanthophores have distinct colors (middle and right panels). (C) Erythrocytes and xanthophores had different spectra under epifluorescence. Erythrocytes autofluoresced in red (displayed in magenta) whereas xanthophores autofluoresced in green. (D) Hue values under brightfield illumination were correlated with ratios of red to green autofluorescence ( $R^2 = 0.92$ ,  $p < 0.0001$ ). (E) Colors of cells varied across the proximodistal axis of the fin, shown as relative position with fin base at 0 and fin tip at 1. Erythrocytes in proximal regions were distinct in both fluorescence ratio and visible hue from xanthophores in distal regions though some intergradation was evident in middle regions, near the melanophore stripe.  $N = 250$  cells from five adult males in D and E. Color fills represent red to green fluorescence ratios. (F) During the larva-to-adult transformation, ratios of red to green autofluorescence diverged between prospective erythrocyte and xanthophore regions. Individual red and yellow points correspond to mean values of cells in proximal and distal regions, respectively, from each of 31 male or female fish ( $N = 620$  cells total) imaged at a range of developmental stages represented by different standard lengths (SL). Scale bars: 5 mm (A, left), 1 mm (A, right); 25  $\mu\text{m}$  (B, C).

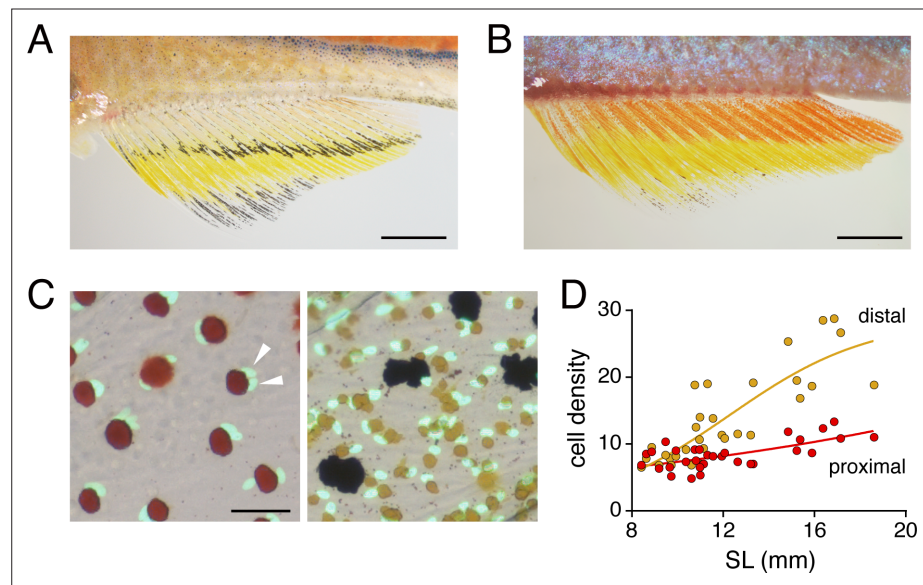


**Figure 2—figure supplement 1.** Sex and age differences in erythrofore pigmentation and occurrence of a binucleated state. **(A)** Erythrofores of female fish were paler than erythrofores of male fish (compare to B and **Figure 2A**). **(B)** Melanophores stripes disappeared in older adult males (compared to **Figure 2A**). **(C)** Erythrofores (left) although not xanthophores (right) were often binucleated, here revealed by transgenic expression of nuclear-localizing *aox5:nucEosFP* (see Main text). Red and yellow pigments had been contracted towards cell centers by epinephrine treatment. Multiple nuclei are indicated by arrowheads. **(D)** Cell densities diverged in proximal and distal regions of the anal fin as fish and fins developed. SL, standard length. Shown are average of cells observed in three regions of  $10^{-2}$  mm<sup>2</sup> prospective erythrofore (proximal) or xanthophore (distal) regions of 31 fish representing a range of stages (N = 620 cells total). Scale bars: 2 mm (**A, B**); 50  $\mu$ m (**C**).

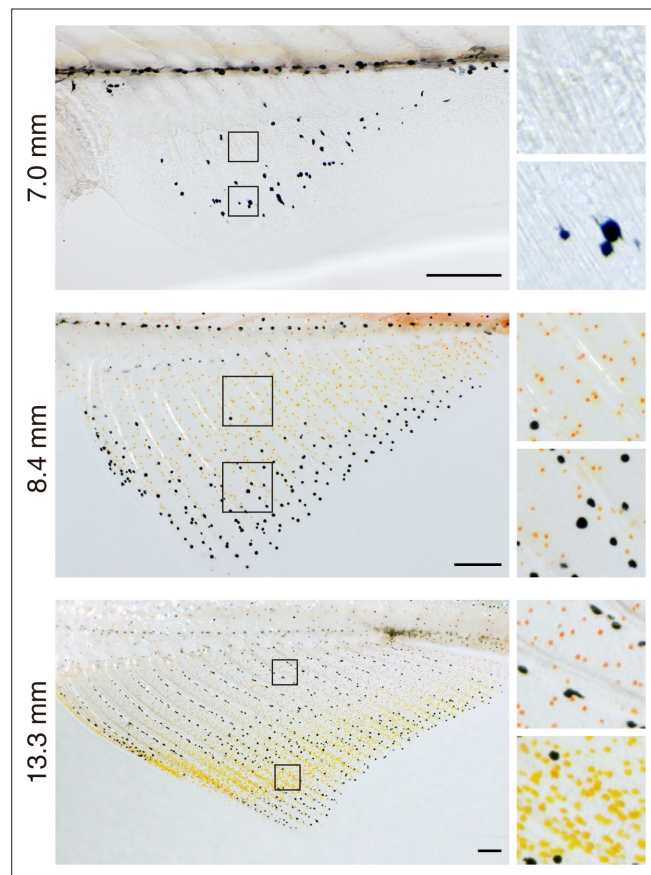


**Figure 2—figure supplement 2.** Pattern development in anal fins of larva to juvenile fish. Melanophores were the first pigment cells evident (7.0 mm SL). Subsequently xanthophore-like cells with orange coloration were found across the fin except in distalmost regions that were enriched instead in melanophores (8.4 mm SL). With additional growth and development, proximal and distal cells diverged in cell color and density (13.3 mm SL), whereas melanophores consolidated into a stripe pattern centrally, as described previously (**Goodrich and Greene, 1959**). Colors of prospective erythrophores and xanthophores were indistinguishable prior to 12 mm SL. Scale bars: 200  $\mu\text{m}$  .

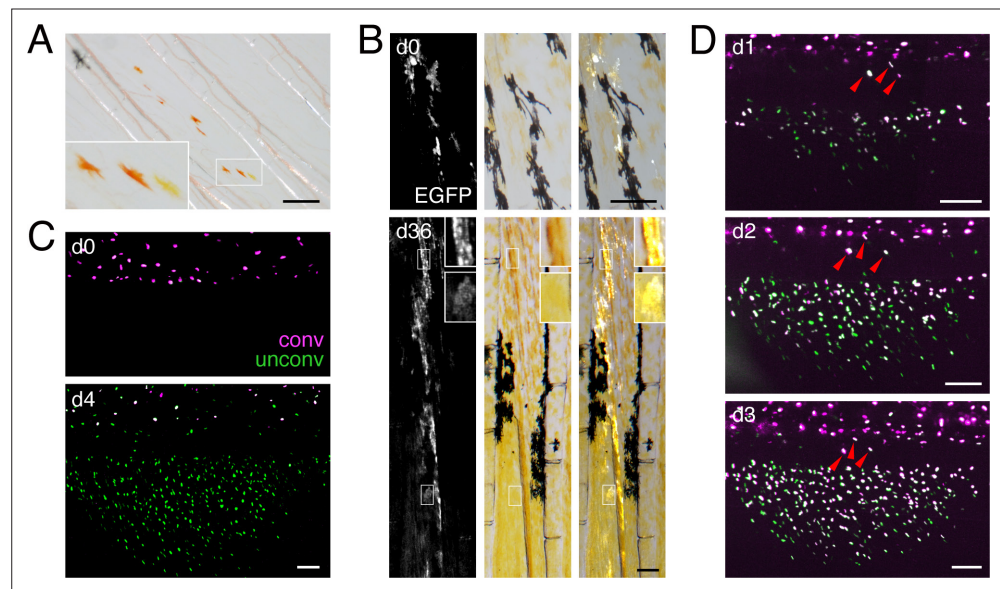


**Figure 3.** Shared progenitor of fin erythrophores and xanthophores revealed by clonal analyses. **(A)** In fish mosaic for somatically induced mutations in *scarb1* most rare, wild-type clones consisted of both erythrophores and xanthophores (8 of 10 presumptive clones in seven fish, with remaining clones only containing one or the other cell type; an additional 56 fish derived from injected embryos either lacked wild-type cells or lacked mutant cells and were thus uninformative). **(B)** Clonal labeling of xanthophores and erythrophores with *aox5:palmeGFP*, illustrating fluorescence, brightfield, and merged views of the same fields. In the clone shown here, an initial complement of several orange cells at the level of the melanophore stripe (d0, 7.5 mm SL) expanded to include more cells proximally and distally to the melanophore stripe that differentiated as erythrophores and xanthophores, respectively (d36, 15 mm SL; red arrowheads). For these analyses, limiting dilutions of *aox5:palmeGFP* were injected into ~500 embryos, yielding 271 embryos that exhibited some fluorescence at 3 days post-fertilization that were further sorted at 16 dpf, identifying 27 individuals with patches of expression in the anal fin. Of these 27 fish, one subsequently died and eight were found to have broad expression across the entire fin, likely representing multiple clones of uncertain boundaries, and so were excluded from analysis. The remaining 18 fish exhibited 24 spatially distinct, presumptive clones of *aox5:palmeGFP*-labeled cells, of which 22 presumptive clones contained both erythrophores and xanthophores as shown here [consistent with mixed clones of melanophores and xanthophores in zebrafish (Tu and Johnson, 2010; Tu and Johnson, 2011)]; one clone contained only erythrophores and one clone contained only xanthophores. **(C)** When *aox5:nucEosFP*<sup>+</sup> cells on the body were bulk photoconverted before fin development, only unconverted *aox5:nucEosFP*<sup>+</sup> cells (green nuclei) were present in the fin 4 days later (images representative of all N = 3 fish tested). **(D)** Successive steps in anal fin development and erythrophore/xanthophore lineage specification revealed many cells newly acquiring *aox5:nucEosFP* expression at daily intervals within the fin (green nuclei). Though some *aox5:nucEosFP*<sup>+</sup> cells were present at the fin base these did not enter into the fin proper (white cells, arrowheads; images shown are from a single individual representative of all N = 7 fish tested in this manner over 23 days each). Scale bars: 200  $\mu$ m (**A**, **B**); 100  $\mu$ m (**C**, **D**).

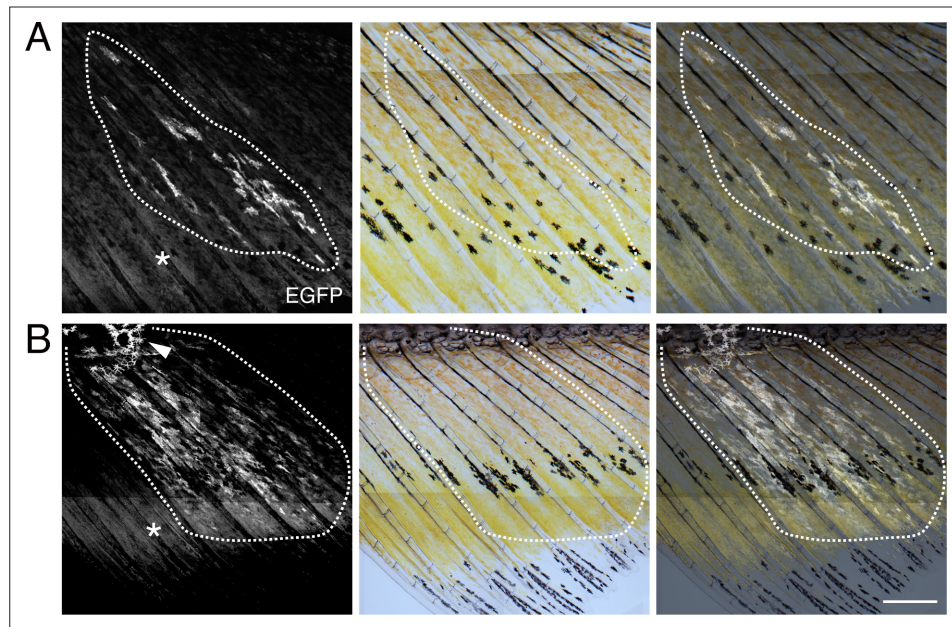


**Figure 3—figure supplement 1.** Transgene labeling of erythrophores and xanthophores. A and B show additional examples of presumptive clones labeled by injection of limiting amounts of *aox5:palmeGFP* transgene. In each individual (36 days, 15 mm SL), EGFP+ cells were found across proximal to distal regions of the fin, contributing to erythrophore and xanthophore populations, respectively. Additional EGFP+ cells were evident on the body at the base of the fin (e.g. arrowhead in B). Asterisks indicate regions of xanthophore autofluorescence in EGFP channel. Images were assembled computationally from tiled acquisitions. Scale bar: 1 mm.

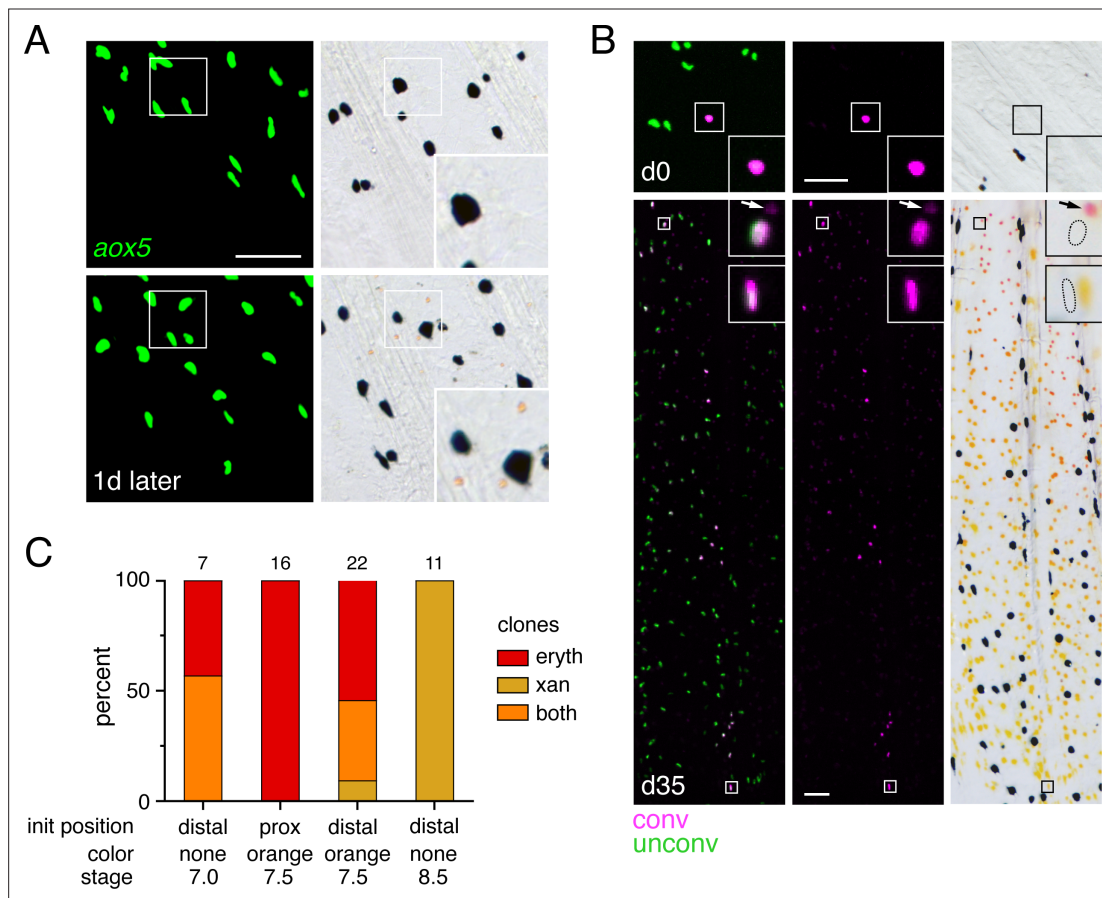


**Figure 4.** Bipotential precursor to erythrophores and xanthophores revealed in the fin by fate mapping. **(A)** Unpigmented cells of the xanthophore lineage, marked by *aox5:nucEosFP* transgene expression (see Main text), present at 7.0 mm SL had acquired a pale orange color 1 day later. (Representative of all N = 7 fish examined by repeated imaging during larval development.) Insets show higher magnification images of a corresponding region. **(B)** Example of a photoconverted, initially unpigmented cell (d0, 7.0 mm SL) that yielded a clone containing both erythrophores and xanthophores (d35, 15.0 mm SL; representative of four of seven clones, with remaining clones containing erythrophores only). Fish were treated with epinephrine to contract pigment before imaging. Arrows indicate erythrophore autofluorescence from red carotenoid pigment, which accumulates adjacent to nuclei following epinephrine treatment; approximate positions of *nucEosFP*+ nuclei in brightfield images are shown with dashed outlines. Insets, proximal and distal cells in the clone. **(C)** Percentages of clones containing only erythrophores, only xanthophores, or both cell types. Numbers above bars indicate clone sample sizes examined. In these analyses pigment cells and progenitors stably expressed *aox5:nucEosFP* (7.5, 8.5 mm SL) or mosaically expressed a different transgene, *mitfa:nucEosFP* (7.0 mm SL), that had been injected into embryos at the one-cell stage. In zebrafish, *mitfa* (*melanophore-inducing transcription factor a*) is expressed by pigment cell progenitors, as well as melanophores and xanthophores (Lister et al., 1999; Budi et al., 2011; Saunders et al., 2019), and we found in *D. albolineatus* that *mitfa:nucEosFP* was expressed in these cells as well as orange cells of larvae and erythrophores of adults. *mitfa:nucEosFP* was used for fate mapping at early stages owing to its more robust expression in unpigmented cells. Scale bar: 50  $\mu$ m.

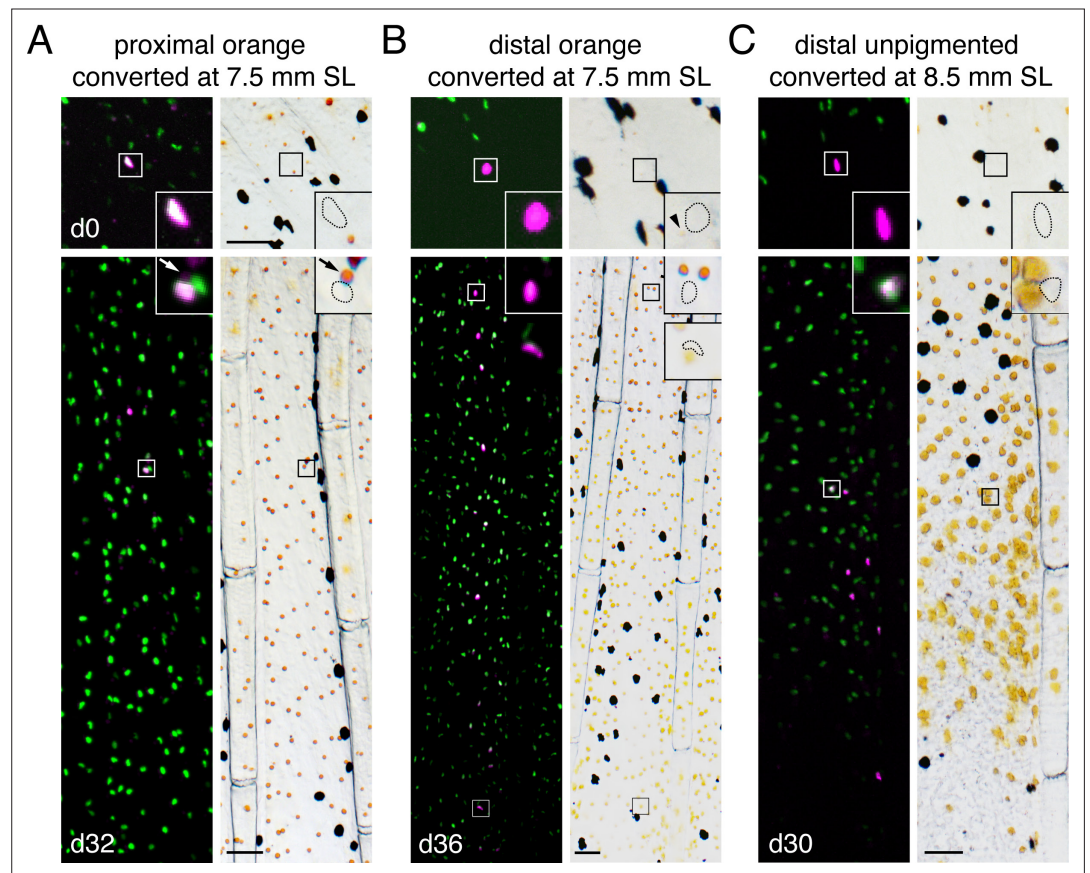


**Figure 4—figure supplement 1.** Fate mapping of single photoconverted cells at different locations and stages. Representative examples of additional classes of clones shown in **Figure 4C**. **(A)** An orange cell initially in the proximal fin that generated daughters remaining proximally developing only as erythrophores. Arrow indicates weak autofluorescence of carotenoid pigment, adjacent to nucleus; approximate positions of nucEosFP+ nuclei in brightfield images are shown with dashed outlines. **(B)** An initially distal cell with pale orange pigmentation (arrowhead) that generated a clone including both proximal erythrophores and distal xanthophores. **(C)** An unpigmented cell at a later stage of fin development initially distal to the melanophore stripe (**Figure 1A**), produced only xanthophores. Scale bar: 50  $\mu$ m.



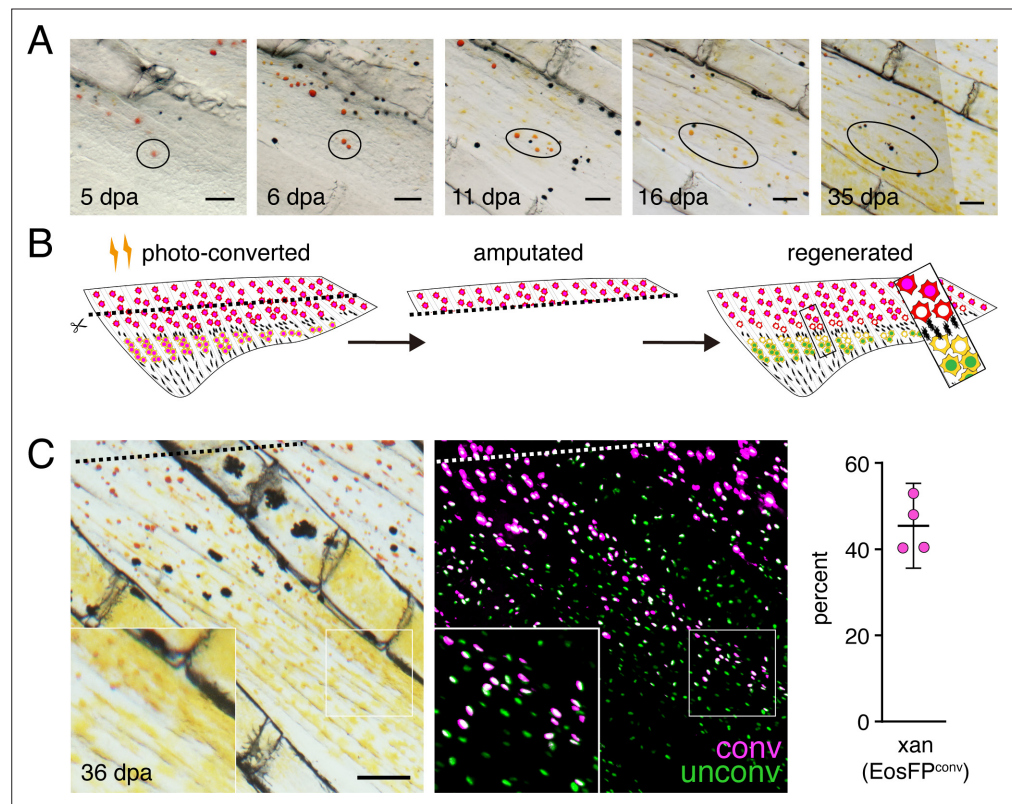


**Figure 5.** Regeneration assays reveal fate plasticity in differentiated cells and latent stem cells competent to differentiate as erythrophores and xanthophores. **(A)** Brightfield sequence of regeneration illustrating apparent conversion of erythrophores to xanthophores (image series representative of all  $N = 3$  fish examined by repeated imaging through regeneration). As fins regenerated, individual erythrophores (circled) near the amputation plane appeared to divide, with presumptive daughter cells having reduced amounts of pigment visible upon contraction with epinephrine and an increasingly yellow–orange color. **(B)** Schematic of regeneration experiment in C. Fins of Tg(*aox5:nucEosFP*) fish were photo-converted *in toto* prior to amputation through the erythrophore region. Fins regenerated over 15 days and pigment pattern had re-formed by 30 days, at which time a new melanophore stripe and distinct regions of erythrophores and xanthophores had developed. **(C)** Example of cells in regenerative tissue 36 days post-amputation (dpa). Regenerative xanthophores near the plane of amputation often contained photoconverted nucEosFP in a region of fin extending 400  $\mu\text{m}$  from the distalmost red erythrophore into the regenerative xanthophore region (means  $\pm$  95 % confidence interval;  $N = 1964$  cells in four fish examined). Dashed lines indicate amputation in B and C. Scale bars: 50  $\mu\text{m}$  (A); 100  $\mu\text{m}$  (C).

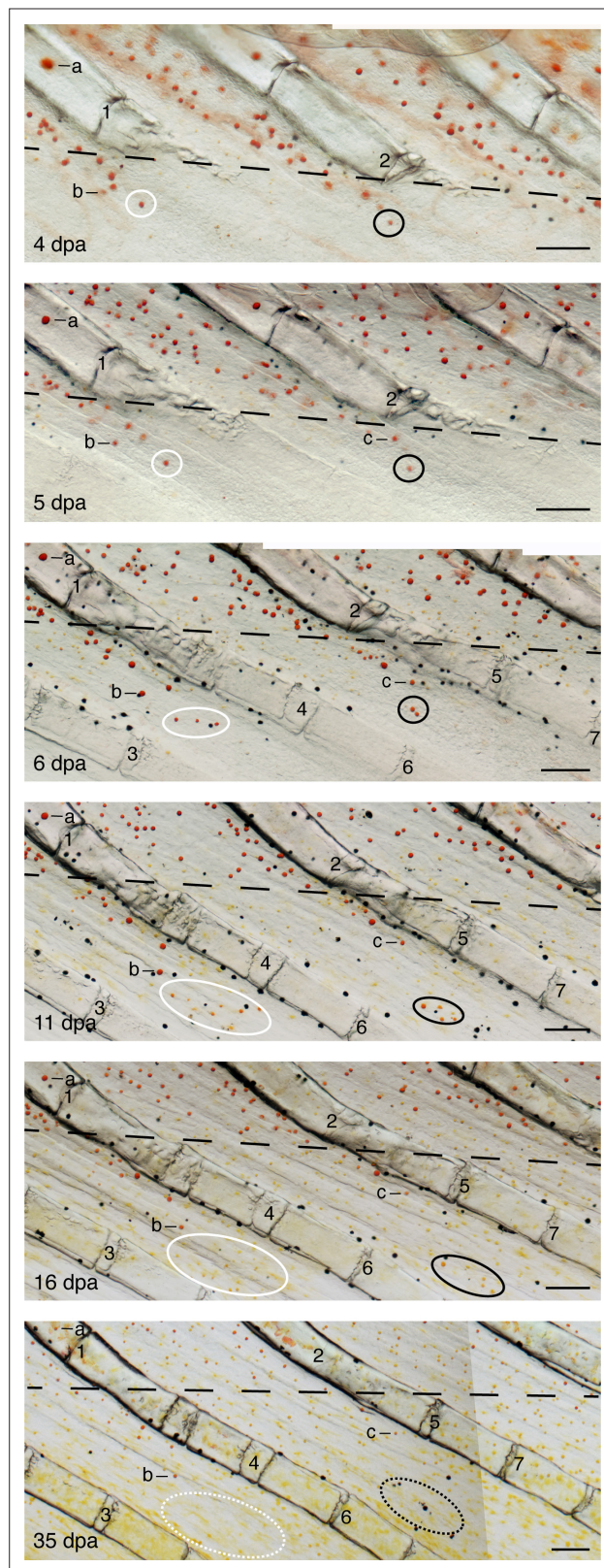


**Figure 5—figure supplement 1.** Pigment cell arrangements and colors and fin tissue context during pattern regeneration. A region of fin is shown at selected time points between 4 and 35 days post-amputation (dpa). Positions of cells that appear to transition from red to yellow are indicated by white and black ovals; approximate positions at 35 dpa are indicated by dashed lines. Several additional erythrocytes are also marked (a–c), as are  
*Figure 5—figure supplement 1 continued on next page*

*Figure 5—figure supplement 1 continued*

morphologically distinguishable fin ray joints (1–7). The amputation plane is marked by a dashed line in each image. Cells marked by the black oval, also shown in **Figure 5A**, become displaced further distally relative to fin ray joints between 6 and 16 dpa. Scale bars: 100  $\mu$ m.

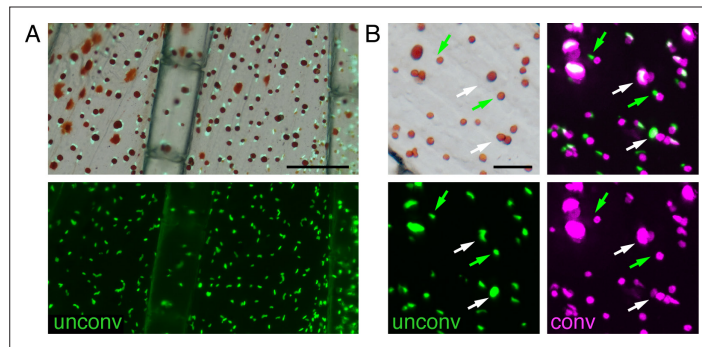


**Figure 5—figure supplement 2.** Regeneration of erythrophores from newly specified unpigmented progenitors. **(A)** Prior to regeneration, only erythrophores expressed *aox5:nucEosFP* in proximal regions; unpigmented *aox5:nucEosFP*<sup>+</sup> cells were not evident, indicating that cells marked by photoconversion post-amputation were derived from previously differentiated erythrophores. Top, brightfield merged with bottom fluorescent image. **(B)** Brightfield and fluorescence (single channel at bottom, merged top right) showing erythrophore nuclei adjacent to contracted pigment granules. Some nuclei retained photoconverted nucEosFP (magenta; white arrows), indicating cells were present prior to amputation, whereas other nuclei were labeled only with photoconverted nucEosFP (green; green arrows), indicating de novo differentiation during regeneration. Newly differentiating erythrophores were rare, however, in this example found only in 2 of 10 interray regions of the fish examined and only in relatively proximal locations. Scale bar: 200  $\mu\text{m}$  **(A)**; 50  $\mu\text{m}$  **(B)**.

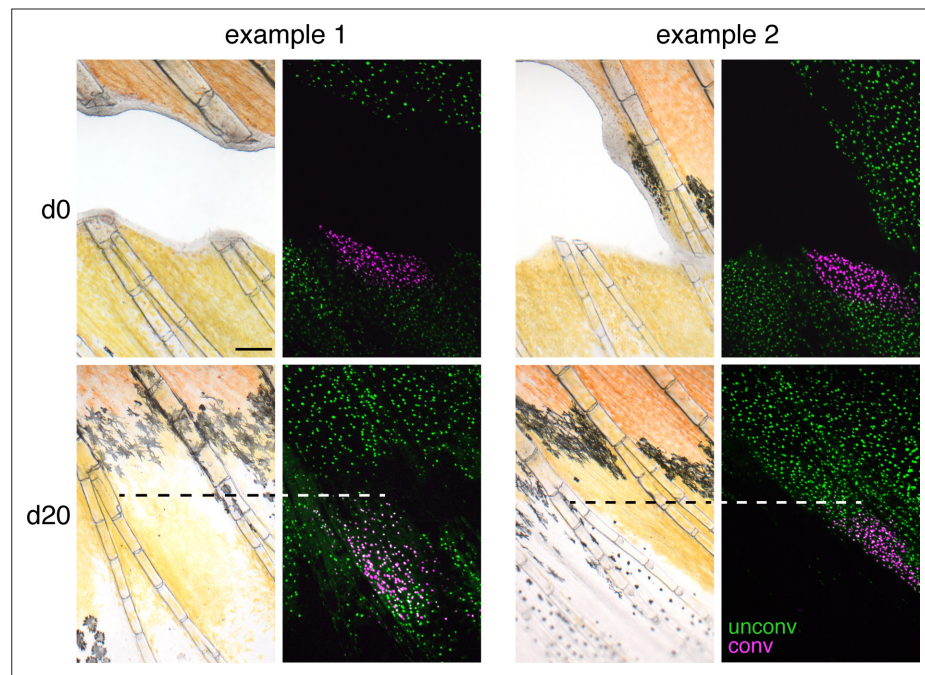


**Figure 5—figure supplement 3.** Regeneration of central fin regions. When internal sections of fin were excised and xanthophores adjacent to the wound marked by photoconversion, these cells or their progeny remained distally and failed to enter more proximal regions where erythrophores regenerated. Two examples of four total fish are shown. Dashed lines, proximal boundary of xanthophores with converted nucEosFP. Scale bar: 200  $\mu$ m.

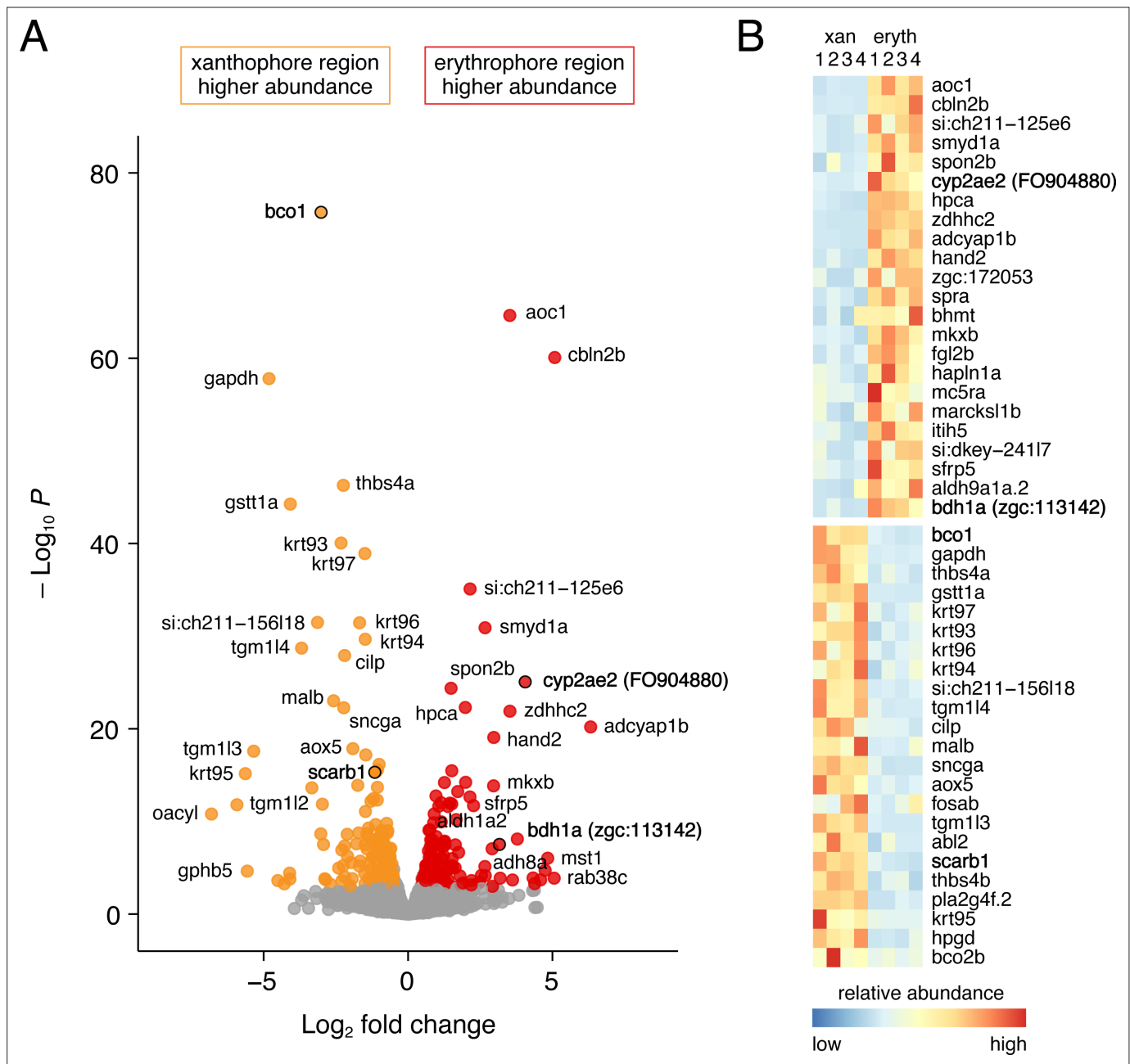


**Figure 6.** Differential gene expression in fin regions with erythrophares and xanthophores. **(A)** Volcano plot of detected transcripts. Yellow–orange and red points indicate transcripts more abundant in xanthophore-containing and erythrophares-containing regions, respectively ( $q \leq 0.05$ ). Gray points, transcripts not significantly different in abundance between regions. **(B)** Heat maps illustrating differential expression of selected loci across fin regions and replicate libraries. Genes with names in bold had phenotypes affecting erythrophares pigmentation.

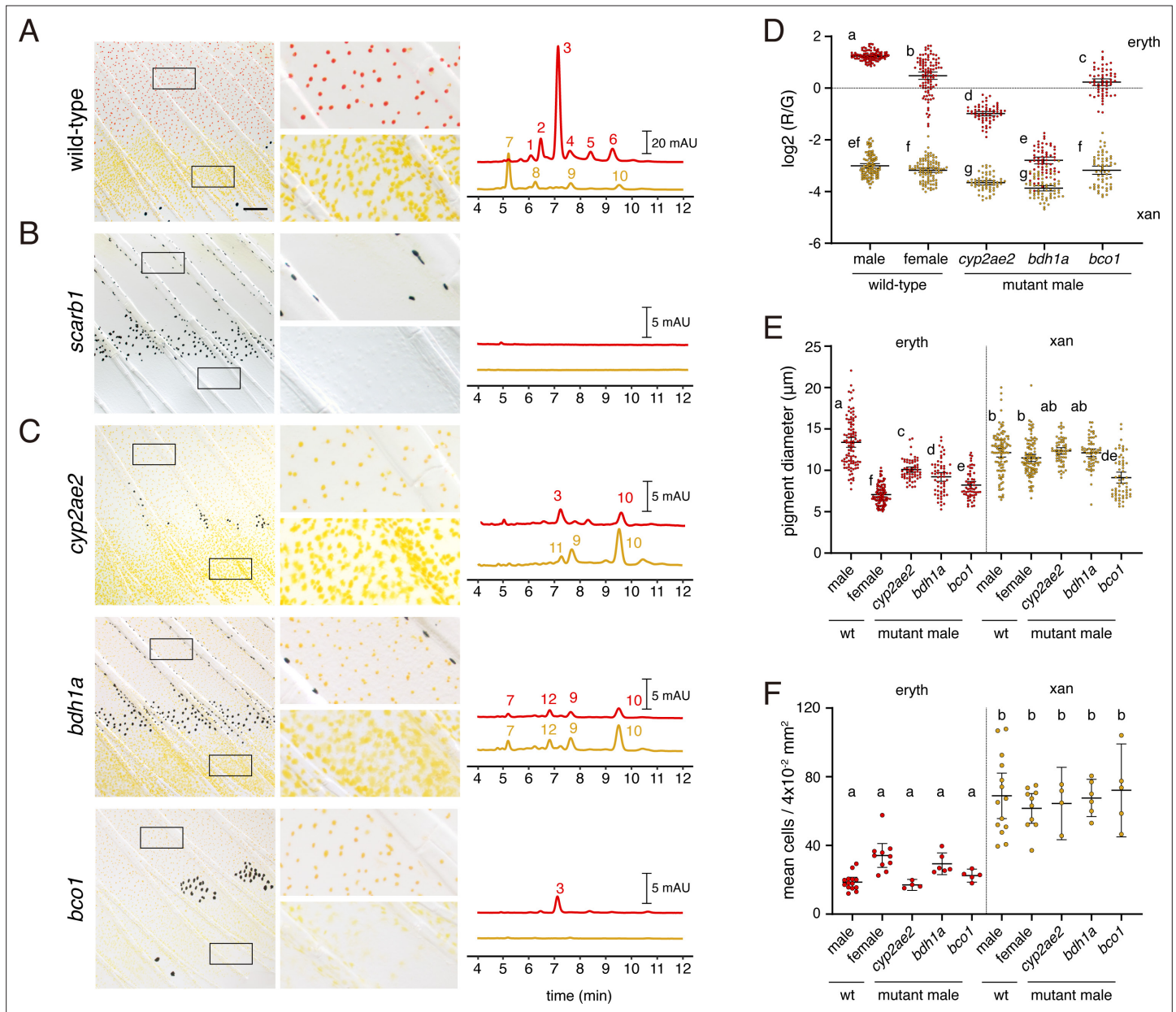


**Figure 7.** Wild-type pigment composition and mutant phenotypes. **(A)** Wild-type fin and carotenoid profile, showing carotenoid absorbance at 455 nm in adult male proximal tissue (red) and distal tissue (yellow). Numbers indicate different carotenoid species, with the most abundant ketocarotenoid in erythrophone-containing tissue being astaxanthin (peak 3; **Figure 1A**; **Figure 7—figure supplement 1**). **(B)** Homozygous *scarb1* mutants lacked red and yellow coloration and carotenoids were not detectable. **(C)** Homozygous mutant phenotypes of genes targeted from RNA-Seq comparisons. *cyp2ae2* and *bdh1a* mutants were deficient for red color and astaxanthin. *bco1* mutants had reduced red and yellow coloration and carotenoids. **(D)** Ratios of red to green autofluorescence for cells found within proximal erythrophone containing regions (red filled points) and distal xanthophore containing regions (yellow filled points) of wild-type males and females compared to mutant males. In the wild-type, erythrophones and xanthophores were segregated into different populations by R/G fluorescence, although differences in females were less marked. In males of each mutant, R/G ratios of erythrophones were reduced compared to wild-type, and lesser reductions were evident in xanthophores (ANOVA, genotype x region interaction,  $F_{4,736}=310.82$ ,  $p < 0.0001$ , after controlling for significant main effects and variation among individuals;  $N = 760$  cells total from five individuals of each background). Plots show means  $\pm$  95 % confidence intervals; means of groups not sharing the same letter differed significantly from one another ( $p < 0.05$ ) in Tukey-Kramer *post hoc* comparisons. **(E)** Wild-type males and females, and mutant males, differed in total visible pigment, as measured by diameters of contracted pigment granules following epinephrine treatment (**Saunders et al., 2019**). (ANOVA, background x region interaction,  $F_{4,736}=76.25$ ,  $p < 0.0001$ , with significant main effects and variation among individuals; diameters were *ln*-transformed for analysis to control for increasing residual variance with means.). **(F)** Densities of erythrophones and xanthophores differed across backgrounds (ANOVA, background x region interaction,  $F_{1,35}=19.01$ ,  $p < 0.0001$ ). Each point represents the mean number of cells counted in three regions of  $4 \times 10^{-2}$  mm<sup>2</sup> in proximal or distal regions with erythrophones or xanthophores, respectively, in each of 39 total fish. Scale bar: 50  $\mu$ m.

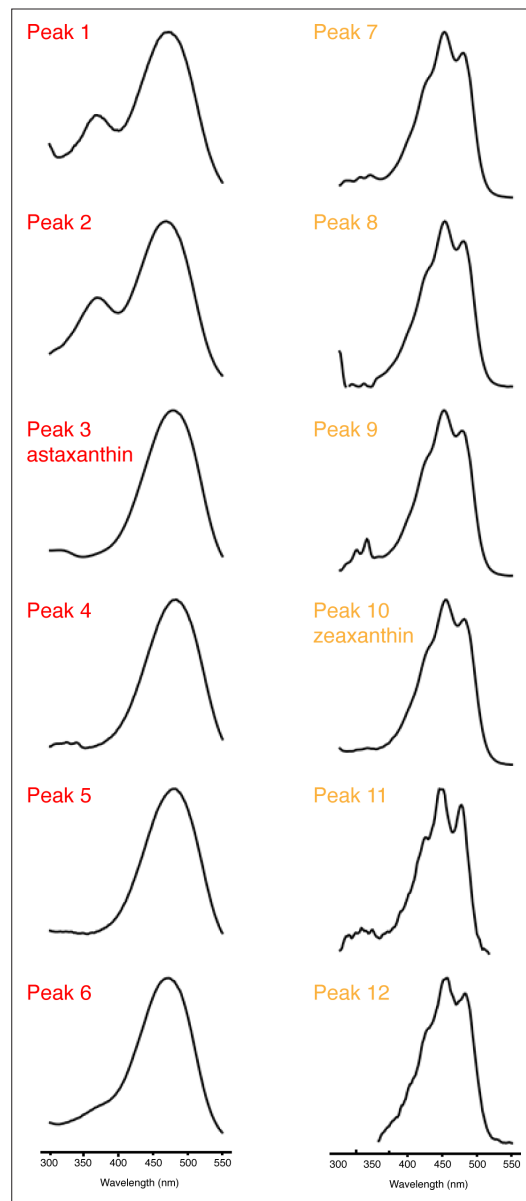


**Figure 7—figure supplement 1.** Characteristics of carotenoid absorbance spectra. Representative normalized UV-Vis absorbance spectra of the major peaks in the carotenoid profiles of red and yellow fin portions of wild-type and various mutant *D. albolineatus* (Figure 7). Peaks 1–6 have a single relatively long-wavelength absorbance peak that is typical of extended conjugated system of C4-ketocarotenoids, including astaxanthin (Peak 3). Peaks 7–12 have multiple smaller peaks characteristic of xanthophyll carotenoids that do not have C4-keto groups contributing the conjugated system, including zeaxanthin (Peak 10).



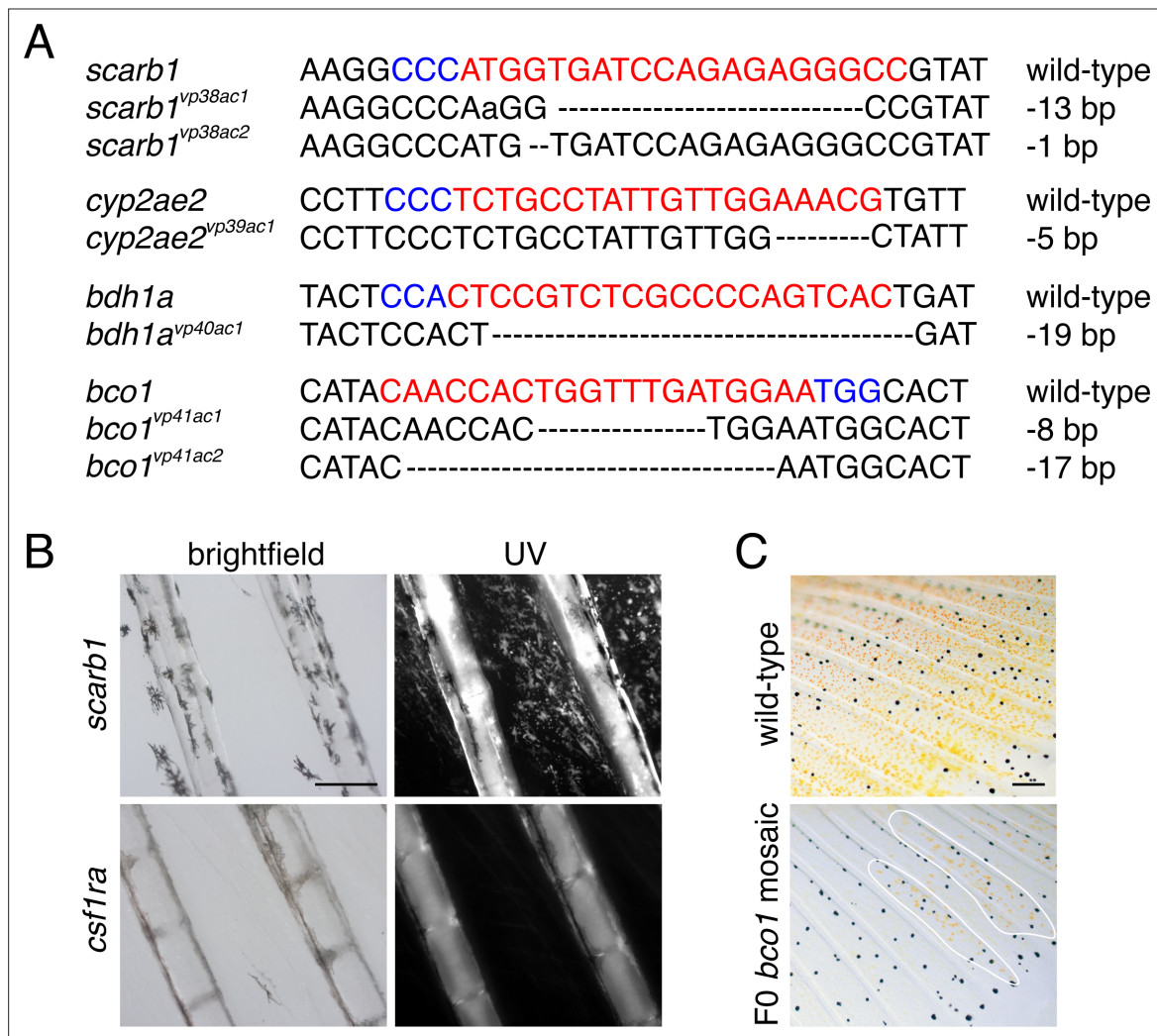


**Figure 7—figure supplement 2.** Mutant lesions recovered, presence of pteridines, and mosaic phenotype of *bco1*. **(A)** Alleles induced by CRISPR/Cas9 targeting of candidate genes. gRNA sequences in red. PAM sequences in blue. Dashed lines indicate missing nucleotides. **(B)** Fish mutant for *scarb1* lacked visible red or yellow color but contained pteridines detectable by autofluorescence under ultraviolet illumination following treatment with dilute ammonia (Odenthal et al., 1996). Pteridine autofluorescence was not present in a xanthophore and erythrophore deficient mutant for colony stimulating factor one receptor a (*csf1ra*) (Lewis et al., 2019), which functions cell-autonomously to promote xanthophore development in zebrafish (Parichy et al., 2000; Parichy and Turner, 2003). **(C)** Carotenoid pigments were mosaic in F0 fish injected with CRISPR/Cas9 targeting *bco1*. Patches of presumably wild-type orange cells are outlined. Scale bar: 200  $\mu$ m.

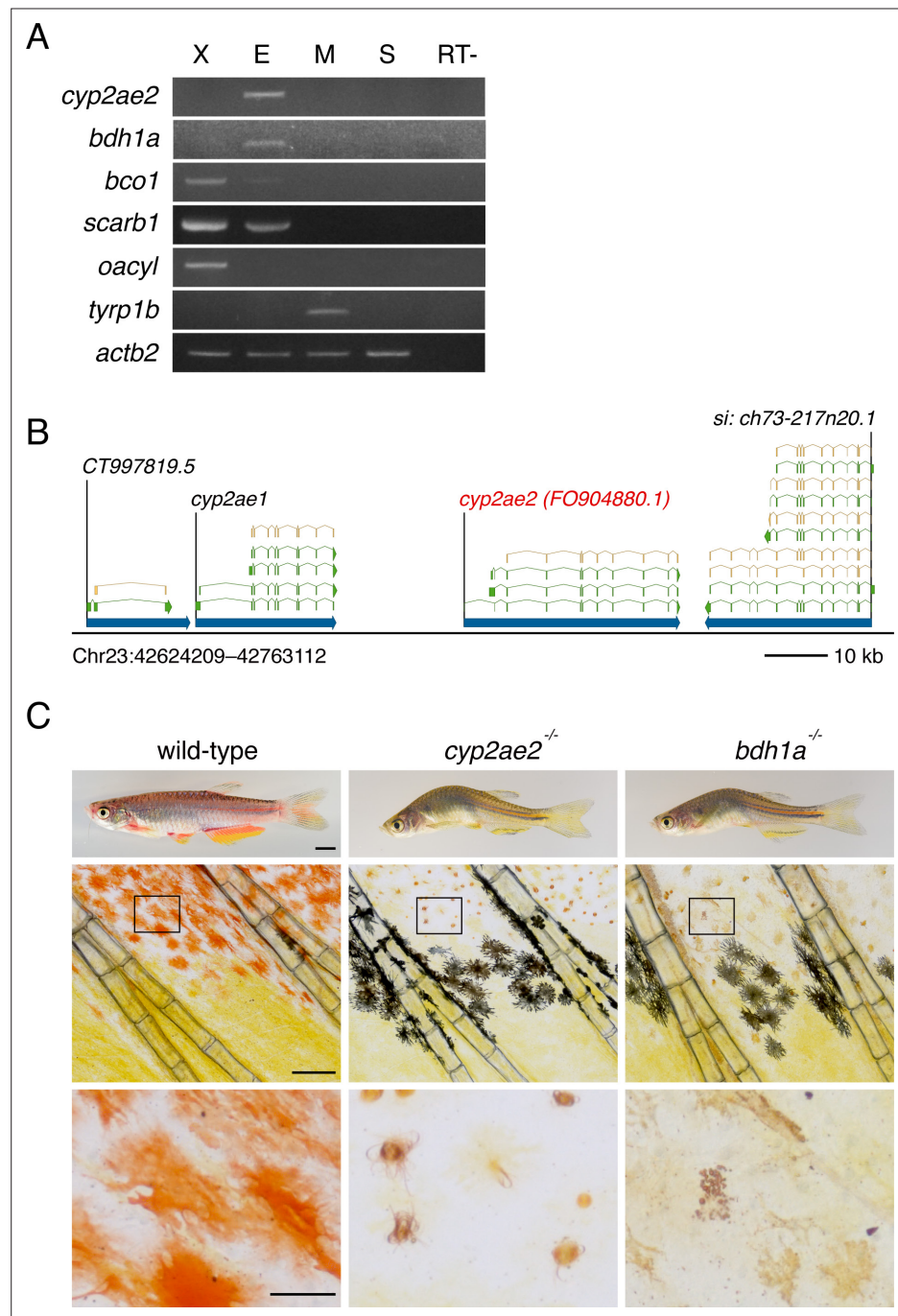


**Figure 7—figure supplement 3.** Expression, genomic location and additional phenotypes of genes contributing to red coloration. **(A)** RT-PCR of isolated pigment cells confirms expression by erythrophores of *cyp2ae2*, *bdh1*, and *scarb1*, and at low levels, *bco1* (X, xanthophores; E, erythrophores; M, melanophores; S, skin; RT-, negative control without reverse transcriptase). *oacyl* and *tyrp1b* mark xanthophores and melanophores, respectively (Saunders *et al.*, 2019); *actb2*, control. **(B)** Genomic context of *cyp2ae2* (FO904880.1) in *D. rerio* GRCz11 (Ensembl Release 103), showing major transcripts (X) and associated coding sequence (tan). **(C)** Later adult pigment cell and body phenotypes of wild-type compared to *cyp2ae2* and *bdh1a* mutants. Scale bar: 4 mm (top); 200  $\mu$ m (middle); 50  $\mu$ m (bottom).